Available online at www.sciencedirect.com
ScienceDirect
Coordination Chemistry Reviews 251 (2007) 492–514
COORDINATION CHEMISTRY REVIEWS
www.elsevier.com/locate/ccr

Review

Application of transient infrared and near infrared spectroscopy to transition metal complex excited states and intermediates

Jennifer M. Butler[a], Michael W. George[c], Jon R. Schoonover[a], Dana M. Dattelbaum[a,*], Thomas J. Meyer[b,**]

[a] *Los Alamos National Laboratory, MS P952, Los Alamos, NM, United States*
[b] *Department of Chemistry, University of North Carolina at Chapel Hill, CB #3290, Chapel Hill, NC 27599, United States*
[c] *School of Chemistry, University of Nottingham, University Park, Nottingham NG7 2RD, UK*

Received 8 July 2006; accepted 5 December 2006
Available online 15 December 2006

Contents

Abstract

Transient infrared spectroscopy (or time-resolved infrared spectroscopy, TRIR) on the nanosecond and faster timescales has continued to evolve as a routine and, sometimes, definitive tool both for elucidation of electronic and molecular structures in metal complex excited-states. This review examines examples from the literature since 1998 and discusses experimental methods for performing transient infrared experiments and recent novel applications of TRIR to the excited states of transition metal complexes. While the interrogation of "reporter" ligands such as ν(CO) and ν(CN) modes in metal carbonyl and cyanide complexes and ν(C=O) ligand modes, has grown extensively toward the identification

* Corresponding author. Tel.: +1 505 667 7329; fax: +1 505 667 6372.
** Corresponding author.
E-mail address: danadat@lanl.gov (D.M. Dattelbaum).

0010-8545/$ – see front matter
doi:10.1016/j.ccr.2006.12.002

of excited states and important features of their bonding, there have been many exciting extensions of the transient infrared technique in recent years. TRIR has been increasingly applied to many types of excited states, resulting in a well-established methodology for assigning excited-state identities. The usefulness of this method has been demonstrated in the unraveling of the sometimes complicated photophysical behavior associated with the complex interplay of multiple excited states, such as closely-spaced MLCT, intra- (IL) and interligand, and dd (ligand-field (LF)) excited states. In recent years, efforts to relate ground-to-excited state vibrational band shifts with other excited state properties (such as the ground-to-excited state energy gap), and medium effects have brought new insights to the understanding of electronic structure in excited states. Application of electronic structure calculations, such as density functional theory approaches, has proven to be a very powerful tool when combined with TRIR in this regard. Relatively new developments, such as non-linear 2D infrared (T2D-IR) spectroscopy, spectroscopic extension into the near infrared, and time-resolved dynamic imaging methods offer exciting possibilities for future applications, and have already presented new capabilities for providing additional insight into the excited states of transition metal complexes.

Keywords: Time-resolved infrared spectroscopy; TRIR; Excited states; Infrared; Transition metal complexes

1. Introduction

One of the most important advances in inorganic spectroscopy over the past 20 years has been the development of time-resolved infrared spectroscopy (TRIR) [1–5]. As applied to transition metal complexes, this technique has been of great assistance in understanding the structures and properties of excited states. It has become an important, often seminal, tool in photochemical and photophysical studies. It has also been effectively applied in other research areas including organic photochemistry, chemical and biological reaction mechanisms, and chemical physics [6].

TRIR has proven to be especially valuable in the study of transition metal complexes containing so-called "reporter" ligands such as CO or CN. Their value in this regard comes from the high oscillator strengths of their stretching vibrations and their π-backbonding relationships with the metal in transition metal complexes. Backbonding makes frequencies and bandwidths of ν(CO) and ν(CN) infrared bands sensitive to changes in electronic and molecular structure. Following metal-based excitation, transient changes occur in these bands on the femtosecond to microsecond timescale. They are often characteristic and can be correlated to changes in electronic structure within the molecule.

More recently, the technique has been applied to ultrafast timescale events, to ring stretching frequencies, and to the near infrared. It has found application in increasingly more complex excited dynamics involving electron transfer, isomerization, and temporal excited-state competitions. The method has also been applied in diverse environments, such as in multiple types of solid matrices and at variable temperatures.

The focus of this review is on recent developments in TRIR (since ~1998) specifically in its application to the excited states of transition metal complexes. Application of TRIR to excited states was initially reviewed in 1993 [7]. A more general review, including application of both TRIR and transient resonance Raman to metal complex excited states, appeared in 1998 [1] and another on TRIR in 1999 [8]. A review in 2000 focused specifically on application of step-scan FTIR in TRIR studies [9].

The emphasis in the early work was on the transient behavior of ν(CO) bands in the 1800–2200 cm^{-1} region. TRIR was used to probe transition metal complex excited states by shifts in reporter ligands, especially ν(CO). The vast majority of studies correlated excited- and ground-state ν(CO) shifts in diimine complexes containing the Os(CO), $Re(CO)_3$, $Re(CO)_2$, and $Ru(CO)_2$ groups having lowest metal-to-ligand charge-transfer (MLCT) excited states. Large, positive ν(CO) shifts were observed characteristic of loss of $d\pi$–π^*(CO) backbonding and strengthening of the CO multiple bond in the excited state.

In particular, early studies focused on complexes containing the $Re(CO)_3$ group because of ease of synthesis and ligand-based "tunability" of excited-state properties. Changes in electron density at the metal in MLCT excited states were inferred from the magnitudes of $\Delta\nu$(CO) shifts with the three ν(CO) normal modes affected differently. Variations in these shifts from complex-to-complex were attributed to the extent of charge transfer to the acceptor ligand.

Electronic origins of excited state(s) were inferred from magnitudes of $\Delta\nu$(CO) shifts. Examples of MLCT, ligand-centered, and $\sigma\pi^*$ excited states were all documented, as well as, examples in which more than one type of state dictated excited-state properties [1].

For complexes containing the $Re(CO)_4$ and $W(CO)_5$ groups, examples were found of lowest ligand-centered excited states and of initial MLCT excited states followed by decay to lower ligand-centered states. Evidence for competing MLCT and XLCT (Halide-to-Ligand Charge Transfer) excited states was found in ruthenium carbonyl halide complexes.

Another area that established the value of TRIR prior to 1998 was use of ν(CO) or ν(CN) shifts to chart excited state intramolecular electron and energy transfer. In multi-site assemblies, application of this technique provided direct evidence concerning the sites involved in excited-state electron or energy transfer. The technique was also applied to non-CO or CN^- containing complexes by monitoring ligand-based bands such as ν(C=O) shifts of carbonyl groups in the fingerprint region, 1650–1400 cm^{-1}.

The focus of this review is on advances, largely in the past six years, of the application of TRIR to transition metal complex excited states. Significant progress has been made during this period through application to new complexes, enhancements in temporal resolution and spectroscopic range, and increasingly sophisticated application of the technique to the unraveling of complex excited-state behavior.

2. Methods

2.1. Step-scan FTIR spectroscopy on the nanosecond to microsecond timescales

Experimental approaches to acquiring TRIR spectra have been discussed elsewhere [1,8,10]. The most common approach on the nanosecond timescale in early applications involved use of a monochromatic IR monitoring source and laser-pulse excitation. "Point-by-point" difference spectra were acquired by repeating the transient measurement at a series of IR frequencies.

Advances in step-scan FTIR spectroscopy [11–13] have provided a more straightforward approach with increased IR throughput and faster data acquisition. Detailed descriptions of this experiment have appeared elsewhere [14,15].

The basis for the step-scan experiment is that the moving mirror of a Michelson interferometer moves in discrete steps. Depending on the instrument, mirror stepping occurs by one of two methods: (1) following a step the mirror is held at a particular mirror position and repetitive excitation with light-on/light-off measurements are made at each position; or (2) the mirror moves continuously with a single light-on/light-off measurement made at each mirror position. The mirror movement is repeated for signal averaging.

The mirror can be held in a stationary position on a pocket of air or "dithered" at a known frequency around a given mirror position. Fig. 1 shows one approach, used by the current authors. In this approach, the infrared light source is directed outside the bench and overlapped with a nanosecond excitation pulse in a purged optical train using of appropriate optics. Changes in infrared absorption are measured with a fast rise time detector and the data manipulated with digital signal processing software in the spectrometer.

A limiting factor in these experiments is that the transient event has to be reproducible at each mirror position. Because of this, the sample under investigation must be stable to multiple excitations or a fresh sample must be continuously added by using flow techniques.

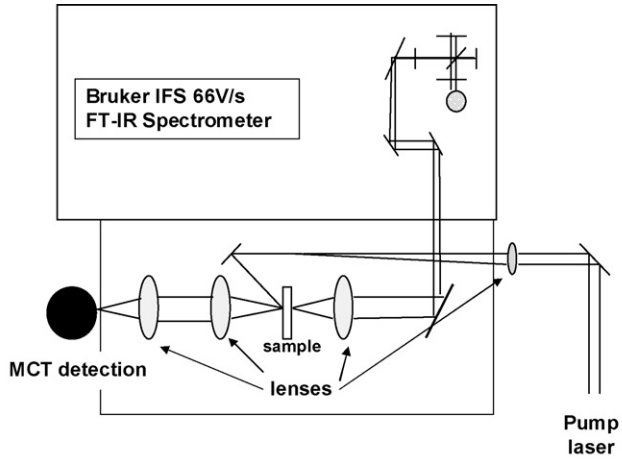

Fig. 1. Step-scan transient FTIR spectrometer for measurements on the nanosecond to microsecond timescales.

2.2. Ultrafast transient infrared methods

Broadband, ultrafast (pico- and femtosecond) TRIR spectroscopy offers an alternative to the nanosecond step-scan method. The major advantage of breaking the nanosecond barrier is a temporal resolution much closer to the initial excitation event. Continuous wave IR sources are not suitable for this application. Pump and probe beams are required that provide ultra-short laser pulses with time resolution achieved by spatially delaying the probe pulse relative to the pump pulse [3].

The IR pulses required for sub-nanosecond TRIR are normally generated from the outputs of commonly available, ultra-short pulsed laser oscillators (Ti-Sapphire oscillator/regenerative amplifier) pumping an optical parametric amplifier (OPA). The signal and idler produced by the OPA are then passed through a $AgGaS_2$ crystal to generate difference frequency mixed, tunable mid-infrared pulses (ca. 150–200 cm^{-1}). Many approaches have been used to detect the transient IR response. Most generally, the IR beams are split to give probe and reference pulses. The pump pulse (visible or UV) is overlapped with the probe pulse in the sample and changes in infrared absorption at various pump-probe time delays are obtained by normalizing outputs from a pair of MCT multi-channel, infrared linear array detectors.

Several approaches have been used to extend transient IR measurements from picoseconds to milliseconds on the same spectrometer including synchronising nanosecond lasers with a ultra-fast laser [16] or two ultra-fast lasers [17]. Synchronising high repetition (1 KHz) nanosecond laser with an ultrafast transient IR laser has produced a highly sensitive spectrometer which can cover a wide range of timescales [18].

2.3. Synchrotron methods

There has also been a growing interest in utilizing synchrotron radiation as the probe for ultra-fast TRIR measurements [19–23]. Synchrotron-produced radiation is achieved at bending magnets by the travel of "bunches" of electrons in a storage ring. It is accessible in short pulses of high brightness in the ps–ns range, and in broad bandwidths (deep UV/X-ray to microwave frequencies). While step-scan methods have approached 1 ns temporal resolution, synchrotron sources offer an advantageous path to sub-nanosecond interrogation of the excited-state dynamics of transition metal complexes. By coupling the short-pulse, broad spectroscopic bandwidth of the synchrotron source with the known advantages of Fourier-transform methods, the adaptability of modern beam lines, and asynchronous sampling, a very attractive approach for sub-nanosecond transient infrared measurements has been achieved. Application of asynchronous sampling in the pump-probe mode is limited by the difficulty in producing the required broadband IR probe pulses. Synchrotron radiation provides such pulses at a sufficiently high repetition rate, pulse width and brightness.

The pump-probe set-up at the National Synchrotron Light Source (NSLS) at Brookhaven National Laboratory utilizes a mode-locked Ti: Sapphire laser as the excitation source, and the synchrotron light source as the probe [19]. Time-resolved

data can be measured as a function of both temperature and frequency. The NSLS facility has also demonstrated a capability for probing the entire spectroscopic range from 2 to 20 000 cm^{-1}. A disadvantage to routine use of the technique is limited access to a synchrotron light source, though most sources are user facilities.

3. Excited states in solution

A major focus of time-resolved infrared studies continues to be identification of excited states. As noted in the Section 1, a proven and powerful method in these studies is the use of reporter ligands which have intense infrared signatures that are sensitive to changes in electron content at the metal or a ligand.

3.1. Reporter ligands and carbonyl mode assignments in Re(pp)(CO)$_3$(L)

Excited states of complexes containing CO and CN^- ligands were among the first to be characterized by TRIR because of high ν(CO) and ν(CN) oscillator strengths and ease of measurement in the 1850–2200 cm^{-1} region. Excited-state shifts occur in ν(CO) and ν(CN) bands in response to electronic redistribution and its influence of dπ–π^*(CO) backbonding.

Fig. 2 illustrates a frontier energy level diagram and MLCT transition accessing the lowest, largely triplet MLCT excited state in a generic *fac*-[Re(pp)(CO)$_3$L]$^{n+}$ complex (pp is a polypyridine ligand such as bpy or phen; L is py, CH_3CN, etc. ($n=1$) or Cl^-, H^-, etc. ($n=0$)). Absorption is dominated by direct excitation to MLCT states largely singlet in character which relax rapidly to lowest-lying, largely triplet states, ^{3}MLCT. Spin-orbit coupling mixes the excited states and direct absorption to ^{3}MLCT can be observed at lower energies.

In the resulting ^{3}MLCT excited states, partial oxidation at the metal reduces available electron density for dπ(Re)–π^*(CO) backbonding. This increases multiple bond character in CO causing a positive $\Delta\nu$(CO) shift in the excited state with shifts

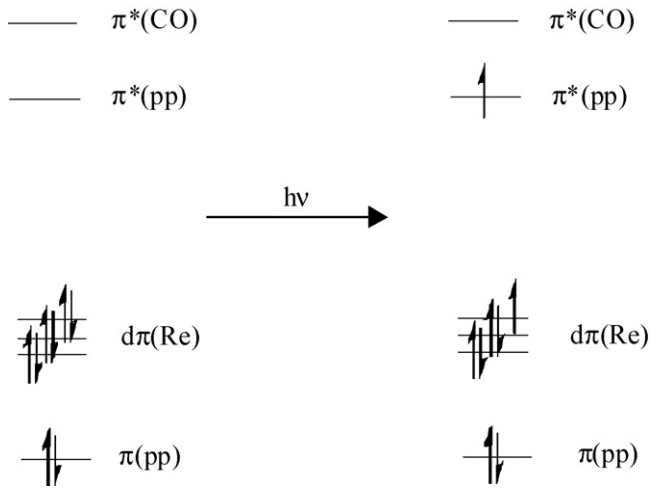

Fig. 2. Frontier energy level diagram for *fac*-[Re(pp)(CO)$_3$L]$^{n+}$ (pp is a polypyridine ligand, L is py, CH_3CN, etc. ($n=1$) or Cl^-, Br^-, etc. ($n=0$)) illustrating MLCT excitation to give the lowest, largely triplet MLCT excited state.

in the range 50–100 cm^{-1} routinely observed. Similar shifts are observed for ν(CN). The magnitudes and directions of these shifts are sensitive to the nature of the excited state.

More detailed analyses point to additional factors that contribute to the magnitude of $\Delta\nu$(CO) [24]. The symmetries of the three ν(CO) modes and their separate shifts reveal additional features about charge redistribution in the excited states [24,25]. In *fac*-[Re(pp)(CO)$_3$L]$^+$ with pp = 2,2′-bipyridine (bpy), or 1,10-phenanthroline (phen) and L = 4-ethylpyridine (4-Etpy), the ground state symmetry is "pseudo-C_{3v}" because of the three facially disposed pyridyl ligands. In this point group, there are three σ_v mirror planes perpendicular to the C_3 rotational axis (z-direction). MLCT excitation promotes an electron to π^*(bpy) or π^*(phen), lowering the symmetry in the excited state to C_s with σ_{xz} the only mirror plane retained.

In C_s symmetry, σ_h, the horizontal mirror plane, is defined as σ_{xy} because there is no C_x rotation axis and σ_h correlates with σ_{xz} in the ground state. The required transformation can be accomplished by rotation around the x-axis. In the new axis system, $\sigma_{xz}=\sigma_h$, but due to the rotation, z in C_{3v} becomes −y, and xz becomes xy. With this transformation, and given the character table for C_s, the A_1 mode in C_{3v} (ground state) becomes A′(y), and E becomes A′(x) and A″(z) (excited state).

Based on this analysis, the ground-to-excited state ($C_{3v}\rightarrow C_s$) correlation of carbonyl modes is $A_1\rightarrow A'(1)$ and $E\rightarrow A''+A'(2)$. The predicted energy ordering for these modes, based on analysis of experimental data and density functional calculations, is $A'(1)>A'(2)>A''$ [26]. The three modes respond differently to substituent changes because of their different local mode compositions [26]. This energy ordering is at odds with an earlier proposal [27], but it was recently confirmed by 2-dimensional (2D) infrared measurements [17].

Transient non-linear 2D infrared (T2D-IR) spectroscopy on the picosecond timescale is a new research area in the field that is gaining interest. 2D-IR is the infrared analogue of COSY and NOESY NMR methods, linking vibrations (and their energies) between ground and excited state(s). T2D-IR extends 2D-IR by offering fast time resolution (picoseconds), and direct information about the coupling of vibrational modes in transient species, which can be used to glean structural information, and link ground-to-excited state shifts. An early example of T2D-IR was in application to a bicyclic octapeptide containing an azobenzene, in which the azobenzene moiety was switched photochemically between *cis*- and *trans*-forms using two different wavelengths. The *cis* → *trans* isomerization takes place within a picosecond with $\Phi\sim0.5$ [28].

Briefly, in the 2D-IR method, a frequency of narrow-band IR as the pump pulse is tuned across a vibrational mode of interest, followed by an IR probe pulse to construct 2D-IR spectra. In T2D-IR, the IR pump pulse is preceded by a UV or visible pulse to excite the complex or molecule of interest. A relevant example mentioned earlier is that of Bredenbeck et al. in the application of T2D-IR to the MLCT excited state(s) of *fac*-[Re(dmb)(CO$_3$)(Cl)] (dmb is 4,4′-dimethyl-2,2′-bipyridine) in DMSO [17]. In this complex, ν(CO) bands are observed in the ground state at 1889, 1910, and 2018 cm^{-1} which are assigned to the A′(2), A″, and A′(1) modes, as described above.

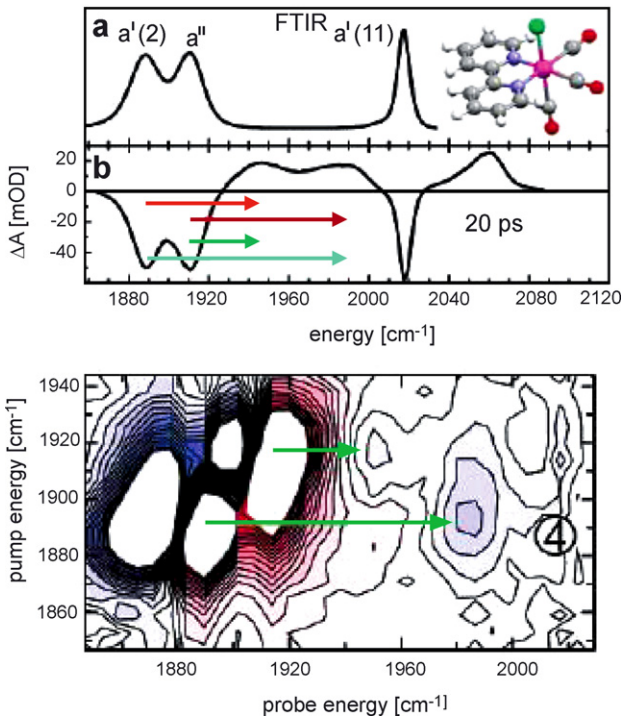

Fig. 3. Transient non-linear 2D infrared (T2D-IR) spectroscopy on the picosecond timescale is analogous to 2-D NMR techniques, in that it "labels" the vibrations of the molecule in the ground state by transferring population from $v = 0$ to $v = 1$, and allows for the correlation of excited state and ground state vibrations by an IR-UV-IR pulse sequence in the 2D spectra. This figure illustrates the application of T2D-IR to the MLCT excited state(s) of [Re(dmb)(CO_3)(Cl)] (dmb is 4,4′-dimethyl-2,2′-bipyridine) in DMSO. In this complex, ν(CO) bands are observed in the ground state at 1889, 1910, and 2018 cm^{-1} which are assigned to the A′(2), A″, and A′(l) modes. By "mapping" the ground-to-excited state shifts in this complex using this novel technique, the change in ν(CO) mode ordering between ground and excited state was confirmed, as predicted by DFT calculations, (excited state ordering A″ < A′(2) < A′(1)) [17,29].

The T2D-IR experiment is well-suited to mapping the shifts of vibrational modes upon excitation to ^{3}MLCT, because it uses 2 IR probes following the UV pump probe to construct a map of ground-to-excited state shifts. It "labels" the vibrations of the molecule in the ground state by transferring population from $v = 0$ to $v = 1$. The excited- and ground-state vibrations are then correlated by an IR–UV–IR pulse sequence in the 2D spectra. Based on the T2D-IR spectrum of *fac*-[Re(dmb)(CO_3)(Cl)] in DMSO in Fig. 3, the ν(CO) modes change their ordering between ground- and excited-state, as predicted by DFT calculations, consistent with the excited-state ordering A″ < A′(2) < A′(1) [29].

3.2. Defining excited states using TRIR

As noted in Section 1, a common application of TRIR has been to aid in the identification of *types* of excited states present following laser excitation, and can be used to support and/or elucidate results obtained by complementary methods such as transient absorption spectroscopy. This is accomplished by using reporter vibrations which respond to electron density changes either at the metal or at a ligand. Qualitative arguments based on band shifts have been buttressed by use of hybrid density functional theory creating a powerful framework for analyzing excited states [29].

MLCT excited states have been studied most extensively. As an example, 354.7 nm excitation of *fac*-[Re^{I}(bpy)$(CO)_3$(4-Etpy)]$^+$ gives the largely triplet MLCT excited state *fac*-[Re^{II}(bpy$^{\bullet-}$)$(CO)_3$(4-Etpy)]$^{+*}$, note Fig. 2. For this complex, ground-state ν(CO) bands at 1927 and 2035 cm^{-1} (E and A_1 in pseudo-C_{3v} symmetry) shift to 1971 cm^{-1} (A″), 2010 cm^{-1} (A′(2)), and 2074 cm^{-1} (A′(1)) with $\Delta\bar{\nu}$(CO) = ($\bar{\nu}_{es} - \bar{\nu}_{gs}$) = +44, +83, and + 39 cm^{-1}, respectively. These band assignments were verified by DFT calculations and confirmed by ultra-fast transient 2D-IR measurements, as mentioned in the previous section [17].

Depending on the ligands, $Re(CO)_3$ complexes are known to have closely-lying MLCT and intraligand $\pi\pi^*$ excited states with a complicated interplay between them. In *fac*-[Re(dppz)$(CO)_3(PPh_3)]^+$ (Ph = phenyl, dppz is dipyrido[3,2-a:2′,3′-c]phenazine) [1,30,31] ν(CO) bands are shifted an average of 8 cm^{-1} to *lower* energy in the excited state (in deaerated CH_3CN) consistent with an intraligand (IL) $^3\pi\pi^*$(dppz) excited state. The lowest-lying π^* orbital on dppz in related Re complexes has been shown by DFT calculations to be largely phenazine-based [1,30,31]. Negative ν(CO) shifts in this, and related complexes, point to a ligand-based triplet excited state that is a worse π-acceptor than the ground state, resulting in more electron density at Re in the excited state compared with the ground state for increased π-backbonding with the carbonyls, and hence lower energy stretching frequencies.

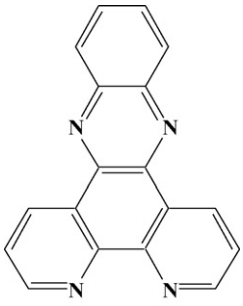

dppz

The lowest-lying excited state in [Pt(dpphen)$(CN)_2$] (dpphen = 4,7-diphenyl-1,10-phenanthroline) has been probed by TRIR both in fluid solution at room temperature and in a 1:1 propionitrile:butyronitrile glass at 77 K [32]. Excited-to-ground state $\Delta\nu$(CN) shifts are less than 5 cm^{-1} to lower energy consistent with a lowest-lying π–π^* intraligand state. By comparison to the carbonyl example described above, $\Delta\nu$(CN) shifts may be expected to be somewhat different than $\Delta\nu$(CO). CN is a better σ-donor, and weaker π-acceptor compared with CO, and $\Delta\nu$(CN) is typically half of $\Delta\nu$(CO) in MLCT excited states. The excited-state shifts for the IL state described here are also slightly smaller for CN compared with the example containing CO above, however the electronic nature of the ligand that the IL state is centered upon will also play a substantial role in the overall electron distribution of the excited state. At 77 K, luminescence is highly structured for [Pt(dpphen)$(CN)_2$], decaying

with $\tau = 170\,\mu s$, also consistent with a ligand-centered excited state. While the $^3\pi\pi^*$ state was confirmed at low temperatures, the authors set out to probe the possible co-existence of a monomer/excimer equilibrium at room temperature. Kinetic analysis of the transient infrared data at room temperature was revealing. At room temperature, kinetic analysis of the decay of the transient at $2145\,cm^{-1}$ (symmetric ν(CN)), and recovery at $2139\,cm^{-1}$ (asymmetric ν(CN)) showed a dominant fast component, and a residual slow component (>20 μs). The concentrations of the two components could be "tuned" with the solution concentration of the complex, consistent with excimer formation and a monomer-excimer equilibrium at room temperature.

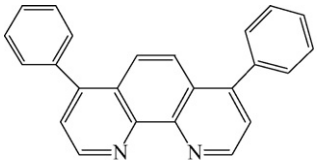

dpphen

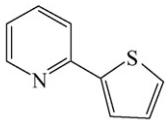

thpy

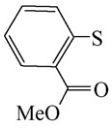

mts

Although few Pt carbonyl complexes have been studied by transient infrared spectroscopy, a cyclometallated Pt(II) thiolate carbonyl complex [Pt(thpy)(CO)(mts)], (thpy = 2-(2′-thienyl)-pyridine, mts = methylthiosalicylate, structures above) has been probed by a combination of cw absorption, emission, and transient (picosecond) TRIR measurements. For both [Pt(thpy)(CO)(mts)] and the related complex [Pt(thpy)(CO)(Cl)], the lowest excited state is predominantly a ligand based $^3\pi\pi^*$ state of thpy. For [Pt(thpy)(CO)(mts)], the single ν(CO) band at $2105\,cm^{-1}$, bleaches and shifts to lower energy in the excited state to $2094\,cm^{-1}$, consistent with a $^3\pi\pi^*$ state. However, a negative solvatochromism of the emission properties of both [Pt(thpy)(CO)(Cl)] and [Pt(thpy)(CO)(mts)] was observed, indicating that the $^3\pi\pi^*$ intraligand state must be mixed with a close-lying state with charge-transfer character. The short lifetime of the intraligand state, 780 ps, points to intervention, and decay through this close-lying excited state, which is probably charge-transfer in origin [33]. Further analysis of this complex molecule, coupling complementary ultra-fast methods (such as TA), and picosecond transient infrared measurements, with electronic structure calculations could be insightful in this case and aid in the unravelling of the interplay of these two states.

Charge- or redox-separated (RS) states have also been identified by TRIR in designed chromophore-quencher assemblies based on *fac*-[Re(pp)$(CO)_3$L]$^+$ sometimes in competition with MLCT or intraligand states. In *fac*-[Re^I(Anqphen)$(CO)_3$(py-PTZ)]$^+$ (Anqphen is 12,17-dihydronaphtho-[2,3-h]dipyrido[3,2-a:2′,3′-c]-phenazine-12,17-dione, py-PTZ is 10-(4-picolyl)phenothiazine), excited-to-ground state $\Delta\nu$(CO) shifts of −6, −3, and $-15\,cm^{-1}$ were observed [34]. MLCT excitation of this complex followed by intramolecular electron transfer results in the redox separated state shown in Eq. (1) as inferred from the TRIR and transient absorption measurements.

$$fac\text{-}[Re^{I}(\text{Anqphen})(CO)_3(\text{py-PTZ})]^+ \xrightarrow{h\nu} fac\text{-}[Re^{I}(\text{Anqphen}^{\bullet-})(CO)_3(\text{py-PTZ}^{\bullet+})]^+ \quad (1)$$

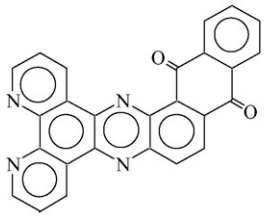

Anqphen

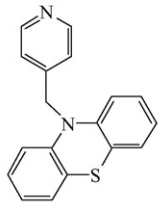

py-PTZ

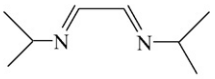

iPr-DAB

The $\Delta\nu$(CO) shifts are of greater magnitude than those for intraligand $^3\pi\pi^*$ states. This was rationalized qualitatively by invoking complete reduction at the Anqphen acceptor ligand which enhanced electron density at Re increasing $d\pi$–π^*(CO) backbonding. The TRIR results were also useful in confirming that complete reduction occurs at the quinone, consistent with EPR results and FMO calculations.

A related example occurs in the excited state(s) of the complex [Pt(bpy)(4-$SC_6F_4CN)_2$]. For this complex picosecond TRIR was used to identify a lowest-lying ligand-to-ligand charge transfer (LLCT) excited state consistent with small, negative $\Delta\nu$(CN) shifts of $\sim -8\,cm^{-1}$ [35]. The HOMO is mainly thiolate-centered with the lowest excited state being [Pt(bpy$^{\bullet-}$)(4-$^{\bullet}SC_6F_4CN$)] in character.

Small positive $\Delta\nu$(CO) shifts are observed for $\sigma\pi^*$ excited states. Following visible MLCT excitation of *fac*-[Re(benzyl)$(CO)_3$(*i*Pr-DAB)] (*i*Pr-DAB is *N*,*N*′-diisopropyl-1,4-diazobutadiene), homolysis of the Re-benzyl bond occurs preceded by $\Delta\nu$(CO) shifts to slightly higher energy consistent with formation of a $\sigma\pi^*$ excited state [36,37]. The small shifts were rationalized by suggesting that promotion of an electron from σ(Re-benzyl) to π^*(DAB) only slightly diminishes $d\pi$–π^*(CO) backbonding.

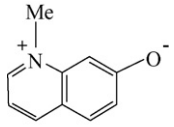

OQD$^-$

Small positive $\Delta\nu$(CO) shifts for *fac*-[Re(4,4′-tBu_2bpy)$(CO)_3$(OQD)$^+$ (OQD is 1-methyl-6-oxyquinoline) in dichloroethane were initially attributed to a $\sigma\pi^*$ excited state [38] but DFT calculations later pointed to $d\pi$–$p\pi_O$ or $d\pi$–π^*(OQD) origins [29]. The smaller positive shifts are a consequence of partial oxidation at Re with the HOMO including both dπ(Re) and $p\pi_O$ character. The lowest energy absorption bands arise from transitions from this HOMO to closely spaced π^*(bpy) and π^*(OQD) levels.

In [Re(phen)$(CO)_4$]$^{+*}$, $\Delta\nu$(CO) shifts were also slightly positive, not those expected for a ligand-centered excited state [9]. The data were interpreted by invoking an admixture of charge transfer character into the nominally ligand-centered excited state.

As noted in the Introduction, TRIR has proven useful in distinguishing between competing ligand field and MLCT excited states in complexes based on $-W(CO)_5$. In this series, MLCT states have large positive $\Delta\nu$(CO) shifts with ν(CO) shifting to lower energy in dd states [7,39]. TRIR

has also been used to investigate ligand-bridged complexes based on $[(CO)_5W(BL)W(CO)_5]$, where BL = pyrazine and 4,4′-bipyridine (4,4′-bpy), in order to investigate electronic distribution in the resulting W^I–W^0 mixed-valence excited states [40]. It was found that the excited state contained IR signatures from the CO ligands attributable to W(0) and W(I) centers and on the IR timescale there was no evidence of delocalization and W(+0.5). Similar studies have been performed on $[Cl(CO)_3Re(BL)Re(CO)_3Cl]$ (BL = 2,3-di-(2-pyridyl)quinoxaline (dpq) and its derivatives [41] with ultra-fast, time-resolved UV-visible and infrared absorption measurements applied to binuclear rhenium(I) polypyridine complexes in solution, or complexes containing dipyrido[2,3-a:3′,2′-c]-6,7-dimethylphenazine [42].

Extension to the fingerprint region has proven challenging due to: (1) low oscillator strengths for the skeletal vibrations that appear in this region; (2) a greater risk of photodecomposition due to the extensive averaging required to overcome poor S/N; (3) spectroscopic congestion causing overlapping ground state bleaches and excited state absorptions; and (4) complexities of interpretation due to the large number of coupled modes which respond differently to changes in electronic configuration between ground and excited states.

Time-resolved resonance Raman (TR^3) has proven effective for characterizing MLCT excited states based on selective resonance enhancement in the reduced, acceptor ligand. In TRIR all infrared active modes contribute to the spectrum. Application to the fingerprint region was successfully applied to the ^{3}MLCT states of $[Ru(bpy)_3]^{2+}$ and $[Ru(phen)_3]^{2+}$ by employing concentrated solutions and extensive signal averaging [43,44]. The features appearing in the resulting difference spectra fell into three categories: (1) ground state bleaches; (2) excited-state absorptions due to ring stretching modes in the non-reduced bpy and phen ligands; and (3) excited-state absorptions in the reduced bpy and phen ligands. Interpretation of the spectra was aided by comparisons with ground-state spectra and spectra of reduced ligands such as $Li^+(phen^{\bullet-})$. Consistent with a conclusion reached earlier based on TR^3 data [45], the TRIR results showed that the excited electron is localized on a single polypyridine acceptor ligand on the IR time scale.

The TRIR technique has also been applied to the series $[Ru(dmb)_3]^{2+}$, $[Ru(dea)_3]^{2+}$, $[Ru(dmb)_2(dea)]^{2+}$, and $[Ru(dmb)(dea)_2]^{2+}$ (dmb is 4,4′-dimethyl-2,2′-bipyridine and dea is 4,4′-bis(dimethylamino)-2,2′-bipyridine [46]. A similar approach to data interpretation led to the conclusion that dmb was the acceptor ligand in all cases consistent with the relative substituent effects of −Me and $-NMe_2$.

Recently, the excited states of $[Ru(bpy)_3]^{2+}$ have been revisited [47], and the data show generally the same IR band positions in the excited state but the relative intensities deviate somewhat from the published results [3], The transient spectrum is shown in Fig. 4. The discrepancies are likely due to the method used to collect the transient data initially. In the initial experiment, data were collected by signal averaging with boxcar integration. This limited time resolution resulting in averaging of a ground state contribution into the excited state. Digital signal processing in current step-scan instruments provides a better approach to acquiring quality spectra.

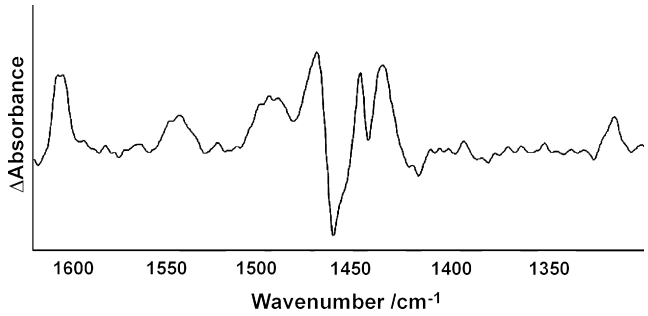

Fig. 4. TRIR spectrum of $[Ru(bpy)_3]^{2+}$ in CH_3CN obtained 100 ns after photolysis [47].

4. Extensions

More recent developments in the application of TRIR to the excited state(s) of transition metal complexes have opened new areas of research and allowed a new set of scientific issues to be explored. Examples include monitoring of temporal TRIR dynamics to elucidate MLCT-induced ligand isomerization and competition between excited states. Qualitative models have also been developed which give insight into the relationship between IR band shifts and excited state electronic structures. The technique is also being increasingly applied to excited-state dynamics in heterogeneous environments such as rigid media and on surfaces.

4.1. Electronic structure

Increasingly quantitative relationships are being drawn between excited-to-ground state IR band shifts and excited-state electronic structure. In one recent study, the ground-to-excited state "energy gap" was shown to play a major role in determining the magnitudes of $\Delta\nu$(CO) shifts. TRIR spectra were obtained for two series, *cis*-$[Os(pp)_2(CO)(L)]^{n+}$ (pp is 1,10-phenanthroline (phen) or 2,2′-bipyridine (bpy); L is PPh_3, CH_3CN, pyridine, Cl^-, or H^-) and *fac*-$[Re(4,4'-(X_2)bpy)(CO)_3(4\text{-Etpy})]^+$ (X is H, Me, OMe, or CO_2Et; 4-Etpy is 4-ethylpyridine) [24]. In both series, systematic variations in $\Delta\nu$(CO) were observed with the excited-to-ground state energy gap, E_0, derived from a Franck-Condon analysis of emission spectra. The energy gap is related to the free energy of the excited state above the ground state, ΔG_{ET} as shown in Eq. (2). In this equation, $\lambda_{o,L}$ is the reorganization energy between excited and ground states arising from the solvent and low frequency vibrations treated classically.

$$E_0 = \Delta G^0_{ET} - \lambda_{o,L} \quad (2)$$

In the Os series, the energy gap was manipulated by varying L through its influence on the dπ(Os) levels. In the Re series, the energy gap was varied by varying the bpy substituent −X with its influence on the π^*(pp) acceptor levels. In both series, large positive $\Delta\nu$(CO) shifts were observed in all cases

Table 1
Ground- ($\bar{\nu}_{gs}$) and excited-state ($\bar{\nu}_{es}$) infrared band energies ($\pm 2\,cm^{-1}$) and shifts ($\Delta\bar{\nu} = \bar{\nu}_{es} - \bar{\nu}_{gs}$), energy gaps ($E_0$), and $E_{1/2}$ values for *cis*-$[Os(pp)_2(CO)(L)]^{n+}$ in acetonitrile at 298 K [24,25]

Complex[a]	$\Delta\bar{\nu}$ (cm^{-1})	$\bar{\nu}_{gs}$ (cm^{-1})	$\bar{\nu}_{es}$ (cm^{-1})	E_0(cm^{-1})[b]	$E_{1/2}(Os^{III/II})$ (V)[c]	$E_{1/2}(bpy^{0/-})$ (V)[c]
cis-$[Os(bpy)_2(CO)(PPh_3)]^{2+}$	42	1975	2017	19200	1.98	−1.09
cis-$[Os(bpy)_2(CO)(CH_3CN)]^{2+}$	68	1979	2047	18400	1.80	−1.14
cis-$[Os(bpy)_2(CO)(py)]^{2+}$	69	1972	2041	17300	1.67	−1.15
cis-$[Os(bpy)_2(CO)Cl]^{+}$	74	1948	2022	14600	1.18	−1.29
cis-$[Os(phen)_2(CO)Cl]^{+}$	75	1950	2025	14800	1.14	−1.24
cis-$[Os(phen)_2(CO)H]^{+}$	76	1911	1987	14000[d]	0.90	−1.43

[a] As PF_6^- salts.
[b] From Table 2.
[c] vs. SSCE.
[d] The emission was too low in energy to fit accurately. The value cited was calculated from the differences between E_{em} values in Table 2.

with the *magnitudes* of the shifts varying with the energy gap. Tables 1 and 2 summarize ground and excited state vibrational energies, $\Delta\nu$(CO) values, E_0 values, and metal and ligand-based reduction potentials.

The trends in $\Delta\nu$(CO) were explained by considering multiple electronic effects, described in more detail in [24,25]. In the Os series, the influence of ground state dπ(M)–π^*(CO) backbonding is key as shown by an increase in $\bar{\nu}$(CO) from 1911 to 1979 cm^{-1} as ancillary ligand L is varied from H^- to PPh_3. The dπ(M)–π^*(CO) energy separation increases in this series decreasing backbonding and increasing $\bar{\nu}$(CO). Variations in excited, $\bar{\nu}_{es}$(CO), and ground state, $\bar{\nu}_{gs}$(CO), band energies are nearly parallel, with $\Delta\bar{\nu}$(CO) constant across the series.

In the Re series, the energy gap was tuned by varying -X in the 4,4′-X_2bpy acceptor ligand. Variations in $\bar{\nu}_{gs}$(CO) due to ground state backbonding are small. All three $\bar{\nu}$(CO) bands shift to higher energy in the MLCT excited states, but in a mode specific manner with $\Delta\bar{\nu}$(CO) largest for the A′(1) mode (Table 2). A pronounced trend was also observed for this series with $\bar{\nu}_{es}$(CO) *decreasing* with *increasing* energy gap, for A′(1) and A′(2). The largest variations with E_o occurred for A′(1). This was attributed to enhanced $\pi^*(pp^{\bullet-})$–π^*(CO) mixing as the $\pi^*(pp^{\bullet-})$ orbital levels are brought closer in energy to π^*(CO). This mixing, facilitated by dπ(Re), provides the orbital basis for mixing π^*(CO)- and π^*(4,4′-X_2bpy)-based MLCT excited states.

Finally, in addition to loss of ground-state backbonding, π(M–CO) bond polarization, and $\pi^*(pp^{\bullet-})$-π^*(CO) mixing as an orbital basis for π^*(CO)- and π^*(4,4′-X_2bpy)-based MLCT excited state mixing, the magnitude and direction of $\Delta\nu$(CO) shifts in these complexes may also be attributed to: (1) σ(M–CO) bond polarization caused by the internal electric field created in the MLCT excited state(s), and (2) dπ(M)–π(pp) mixing. The latter provides an orbital basis for mixing $\pi\pi^*$- and π^*(4,4′-X_2-$bpy^{\bullet-}$)-based MLCT states.

In a recent extension, picosecond TRIR, TR^3, and UV-visible measurements have been reported on *fac*-[Re(dmb)$(CO)_3$(4-Etpy)]$^+$and *fac*-[Re(bpy)$(CO)_3$Cl]. TRIR measurements of ν(CO) bands offered insight into the evolution of vibrational mode shifts at very early times. Time-dependent blue shifts and band narrowing occurred between 1 and 11 ps. The early-time transient behavior was attributed to cooling of anharmonically-coupled low frequency modes [48]. Band evolution was complete with thermal equilibration by 100 ps with results obtained consistent with earlier nanosecond measurements.

4.2. Coupling of TRIR and density functional theory calculations

In recent years, density functional theory (DFT) calculations have been used as a tool for characterizing excited-state electronic and molecular structure. DFT calculations of vibrational frequencies are inherently limited by their assumption of harmonic potential functions. This results in calculated frequencies that are scaled and their identification with particular normal

Table 2
Ground- ($\bar{\nu}_{gs}$) and excited-state ($\bar{\nu}_{es}$) infrared band energies ($\pm 2\,cm^{-1}$) and shifts ($\Delta\bar{\nu} = \bar{\nu}_{es} - \bar{\nu}_{gs}$), energy gaps ($E_0$), and $E_{1/2}$ values for *fac*-$[Re(pp)(CO)_3(4\text{-Etpy})]^+$ in acetonitrile at 298 K [24,25]

Complex[a]	$\Delta\bar{\nu}$ (cm^{-1})			$\bar{\nu}_{gs}$ (cm^{-1})		$\bar{\nu}_{es}$ (cm^{-1})			E_0 (cm^{-1})[b]	$E_{1/2}(Re^{II/I})$ (V)[c]	$E_{1/2}(bpy^{-/0})$ (V)[c]
	A′(2)	A″	A′(1)	*E*	A_1	A′(2)	A″	A′(1)			
$[Re(phen)(CO)_3(4\text{-Etpy})]^+$	31	80	26	1931	2036	1962	2011	2062	18300	1.83	−1.03
$[Re(4,4'\text{-}(CH_3)_2bpy)(CO)_3(4\text{-Etpy})]^+$	37	81	33	1927	2034	1964	2008	2067	18700	1.78	−1.16
$[Re(4,4'\text{-}(CH_3O)_2bpy)(CO)_3(4\text{-Etpy})]^+$	41	87	37	1921	2033	1962	2008	2070	18000	1.75	−1.19
$[Re(bpy)(CO)_3(4\text{-Etpy})]^+$	44	83	39	1927	2035	1971	2010	2074	17900	1.74	−1.17
$[Re(4,4'\text{-}(CO_2Et)_2bpy)(CO)_3(4\text{-Etpy})]^+$	45	88	54	1933	2038	1978	2023	2092	16200	1.89	−0.77

[a] As PF_6^- salts.
[b] From Table 4.
[c] vs. SSCE.

modes in the absence of isotopic exchange data can be problematical. Nonetheless, when coupled with TRIR, they have provided new insights into metal complex excited states [49–51].

An example is application of DFT to the two series *cis*-$[Os(pp)_2(CO)(L)]^{n+}$ and *fac*-$[Re(pp)(CO)_3(4\text{-Etpy})]^+$ mentioned in the previous section [24,29]. Calculations on the ground and lowest triplet excited states of *fac*-$[(bpy)Re(CO)_3(4\text{-Etpy})]^+$ led to revision of earlier assignments of ν(CO) energy ordering in the excited states to: $A'(1) > A'(2) > A''$. The $A'(1)$ and $A'(2)$ modes were shown to be most sensitive to variations in the energy gap because they have significant equatorial character and dominate $\pi^*(pp^{\bullet-})$-π^*(CO) mixing in the excited states. These calculations also provided explanations for the relative intensities of the $A'(2)$ and A'' excited-state bands and for the large $\Delta\nu$(CO) shift for $A'(2)$, and for its relative insensitivity to variations in -X.

The combined TRIR/DFT approach was extended to molecular assemblies containing appended electron-transfer donors or acceptors with ligand structures illustrated in Section IIIb [29,52]. As noted there, the lowest excited state in *fac*-$[Re(4,4'\text{-}(CH_3)_2bpy)(CO)_3(OQD)]$ was shown to be $d\pi p_\pi(O)$–$\pi^*(pp)$ in character rather than $\sigma\pi^*$. In these calculations, intraligand $\pi \rightarrow \pi^*$ MLCT, intramolecular $d\pi p_\pi(O)$–π^*, and redox-separated (RS) states were all taken into account. Calculated $\Delta\nu$(CO) shifts compared well with experiment. In *fac*-$[Re^I(dppz)(CO)_3(py\text{-}PTZ)]^+$, DFT calculations confirmed the close energy ordering between RS ($dppz^{\bullet-}$-$PTZ^{\bullet+}$) and $\pi\pi^*$ states observed experimentally.

The mechanism of photochemical ligand substitution of *fac*-$Re(bpy)(CO)_3(PR_3)]^+$ have been examined by TRIR and shown that the ^{3}LF excited state(s) are thermally accessible from ^{3}MLCT [53]. Competition between MLCT and LF excited states was observed in the series [54] and $[W(CO)_4(N,N'\text{-bis-alkyl-}1,4'\text{-diazabutadiene})$ and investigated by DFT and picosecond TRIR [55–57]. The experimental measurements revealed a lowest-lying $d\pi$–π^*(CO) MLCT excited state in contrast to earlier assumptions that the lowest state was metal centered. The DFT calculations reinforced this conclusion and showed that lowest-lying $d\pi(W(CO_{eq})_2) \rightarrow \pi^*(CO_{ax})$ MLCT to CO excited states are a common feature in the series *cis*-$[M(CO_4L_2]$, M = Cr, Mo, or W. The theoretical analysis was extended to assess the relative roles of W → L and W → CO MLCT and W-localized LF excited states [56].

In a recent application, DFT and ps-TRIR were applied to the low-lying excited states and primary photoproducts of $[Os_3(CO)_{10}(s\text{-}cis\text{-}L)]$ (L = cyclohexa-1,3-diene, buta-1,3-diene) [58]. In this study, lowest-lying absorptions probed by 430 nm excitation were assigned to σ(core) → π^*(CO) transitions with the lowest-lying excited state having $\sigma(Os_1\text{-}Os_3)$-π^*(CO) character. DFT calculations were used to determine the optimized geometry of the cluster and to identify the lowest energy electronic transitions. The HOMO is principally localized at metal centers in the cluster core. The LUMO includes orbital contributions at all of the bound carbonyls and the diene ligand. In this example, transient infrared on the picosecond timescale was essential for guiding the theory calculations and aiding in the assignment of the photoproduct to a CO-bridged species. A broad bleach appeared at ca. 2110 cm^{-1} with contributions to the spectrum from a multi-featured transient at lower energies. The overlap of multiple infrared bands at pump-probe delays of 0 to 500 ps, made assignment of the excited-state ν(CO) band energies unattainable. Though the transient spectrum was complex, sustained photolysis gives the photoproduct $[Os_3(CO)_8(\mu\text{-}CO)_2(cyclohexadiene)]$ with two easily-identifiable CO bridges formed in a step-wise fashion as monitored by ps-TRIR. Irradiation of the complex at lower energy was accompanied by bleaching of the 2011 cm^{-1} vibration, and a growth of a CO band shifted to lower energy (2090 cm^{-1}) compared with the ground state, consistent with an decrease in the CO bond order, and population of a predominantly $\sigma \rightarrow \pi^*$ excited state. Following excitation at 400 nm and monitoring in the 1900–1750 cm^{-1} region, it became clear that a μ-CO bridge is formed, as evidenced by a rapidly-appearing band at 1815 cm^{-1} (t = 0–3 ps) that evolves into two other bands at 1801 and 1815 cm^{-1}, associated with two new, but different, μ-CO "bridges" at longer pump-probe delay times. Concurrent with the formation of the two-μ-CO-bridged complex, the higher frequency band near 2100 cm^{-1} shifts in the positive direction to 2106 cm^{-1} consistent with decreased backbonding in the terminal carbonyls, due to the more strongly π-accepting bridging carbonyls pulling electron density from Os.

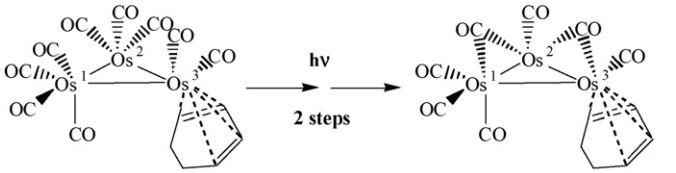

$[Os_3(CO)_{10}(s\text{-}cis\text{-}L)]$ — secondary photoproduct as predicted by TRIR and DFT

The combination of DFT calculations and TRIR has been applied to CO dissociation in the series *trans*(X,X)-$[Ru(bpy)(CO)_2(X)_2]$ (X = Cl, Br, I) [59]. Analysis of the DFT calculations leads to the conclusion that the lowest-lying singlet excited states are of mixed X → bpy/Ru → bpy (LLCT/MLCT) character. Comparison between DFT calculations and TRIR results were used to identify excited states and photochemical intermediates.

4.3. Assemblies

DFT calculations have also been useful to help elucidate photochemical and photophysical properties of supramolecular assemblies. Their architectures are often inspired by attempts to mimic the functional elements of the reaction center of photosynthesis. Examples include the assemblies *fac*-$[Re^I(4,4'\text{-}(CH_3)_2bpy)(CO)_3(OQD)]$ and *fac*-$[Re^I(dppz)(CO)_3(py\text{-}PTZ)]^+$ mentioned above [41,60,61]. These assemblies are typically designed to promote electron or energy transfer following photoexcitation. TRIR has become a, sometimes, definitive tool for elucidating mechanism.

In one early study TRIR was applied to the MLCT excited states of $[(4,4'\text{-}(X)_2bpy)(CO)_3Re^I(4,4'\text{-bpy})Re^I(CO)_3(4,4'\text{-}(X)_2bpy)]^{2+}$ (X = H, CH_3; 4,4′-bpy is 4,4′-bipyridine) [62].

Based on TR[3] and TRIR results, 4,4′-bpy was shown to be the acceptor ligand in $[(dmb)(CO)_3Re(4,4'\text{-}bpy)Re(CO)_3(dmb)]^{2+*}$ (dmb = 4,4′-$(CH_3)_2$bpy)) with MLCT excitation giving the mixed-valence MLCT excited state $[(dmb)(CO)_3Re^{I}(4,4'\text{-}bpy^{\bullet-})Re^{II}(CO)_3(dmb)]^{2+*}$. A solvent dependent equilibrium between 4,4′-bpy and 2,2′-bpy as acceptor ligands occurs in $[(bpy)(CO)_3Re(4,4\text{-}bpy)Re(CO)_3(bpy)]^{2+*}$ as shown by TRIR measurements.

In a related study TRIR ν(CO) measurements were used to ascertain the lowest MLCT excited states in the isomeric ligand-bridged complexes, $[(bpy)_2Ru^{II}(AB)Re^{I}(CO)_3Cl]^{2+}$ (Ru(AB)Re), and $[(CO)_3ClRe^{I}(AB)Ru^{II}(bpy)_2]^{2+}$ (Re(AB)Ru) (AB is 2,2′:3′2″:6″,2″-quaterpyridine) [63].

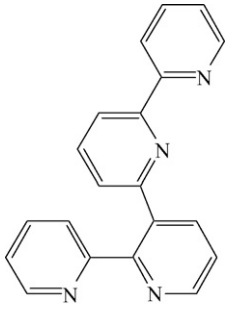

AB

TRIR has been applied to energy transfer in oligomeric assemblies in which MLCT complexes are linked through an oligomeric backbone or through bridging ligands. An example based on conjugated phenylethynylenes (OPEs) from the work of Schanze and co-workers, is shown in Fig. 5.

TRIR measurements revealed low-lying $d\pi(Re) \rightarrow \pi^*(OPE)$ MLCT and $^3\pi,\pi^*(OPE)$ excited states with the latter dominant as shown by TRIR [64]. UV/visible spectra are dominated by two intense $\pi \rightarrow \pi^*$ bands near 335 nm arising from long- and short-axis transitions within the oligomer chain. MLCT absorptions are overlapped and do not appear as separate features in the spectra [65].

The band width for $\pi \rightarrow \pi^*$ emission at $\lambda_{em} \sim 650$ nm decreases with increasing chain length. This is due to a decrease in electron-vibrational coupling with increasing delocalization. MLCT emission, which occurs on the low-energy side of the $\pi\pi^*$ emission, increases with decreasing temperature pointing to more efficient $\pi\pi^* \rightarrow$ MLCT energy transfer [65].

Decreasing solubility for longer chain oligomers limits application of TRIR but CCl_4 was used successfully to explore the effect of oligomer length. It offers the additional advantage of optical transmissibility over most of the infrared. In ground-state spectra the A′, A′(1) and A′(2) ν(CO) modes of C_s symmetry appear with band energies nearly constant across

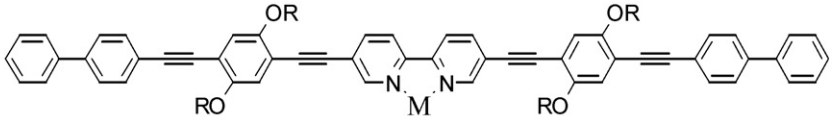

5-Re-2

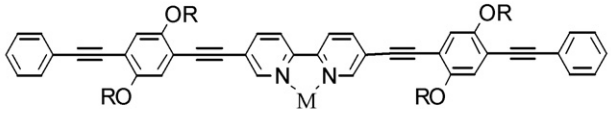

5-ReP-2

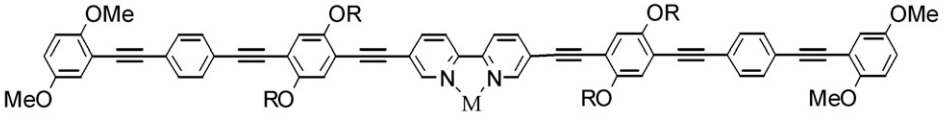

5-ReP-3

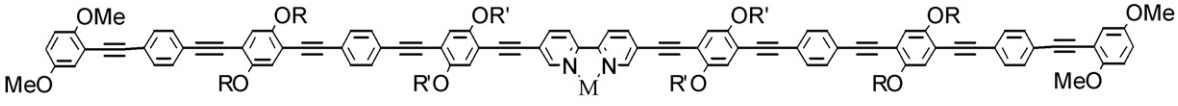

5-ReP-4

R = $C_{18}H_{37}$
R' = C_7H_{15}
M = $Re(CO)_3Cl$

Fig. 5. π-Conjugated phenylacetylene oligomers substituted with (5,5′-X_2bpy)$Re(CO)_3Cl$.

Table 3
Summary of TRIR results in CCl_4 for the series of π-conjugated phenylacetylene oligomers shown in Fig. 5 at 298 K. $\bar{\nu}_{gs}$, $\bar{\nu}_{es}$, and $\Delta\bar{\nu}(=\bar{\nu}_{es}-\bar{\nu}_{gs})$ are the ground and excited state ν(CO) band energies and excited-to-ground state Δν(CO) shifts

Oligomer	$\bar{\nu}_{gs}$ (cm^{-1})	$\bar{\nu}_{es}$ (cm^{-1})	$\Delta\bar{\nu}$ (cm^{-1})
5-Re-2	2024	2009	−15
	1929	1921	−8
	1907	1900	−7
5-ReP-2	2024	2003	−21
	1930	1916	−14
	1908	1887	−21
5-ReP-3	2024	2007	−17
	1926	1917	−9
	1906	1896	−10
5-ReP-4	2025	2011	−14
	1930	1921	−9
	1913	1898	−15

the series, Table 3. Excited-state ν(CO) bands are shifted to lower energy consistently throughout the series. For example, for the oligomer labeled 5-Re-2 in Fig. 5, ground-state bands at 1907, 1929 and 2024 cm^{-1} bleach with new bands appearing to lower energy at 1900, 1921, and 2009 cm^{-1} with Δν(CO) shifts of −8 cm^{-1} (A′(1)), −10 cm^{-1} (A″), and −15 cm^{-1} (A′(2)). The shifts to lower energy are remarkably similar to shifts in *fac*-[Re(dppz)(CO)$_3$(PPh$_3$)]$^{+*}$ in which the excited state is $^3\pi\pi^*$(dppz). This observation points to lowest-lying oligomeric $\pi\pi^*$ excited states in the series in Fig. 5 as well.

The negative shifts and increase in dπ–π* backbonding are due to increased π*(oligomer)-π*(CO) mixing via the dπ(Re^I) orbitals. Based on Δν(CO) shifts, the extent of π*(oligomer)-π*(CO) mixing does not appear to change significantly across the series in Table 3. This indicates a possible broken π conjugation in the oligomer. Increasing delocalization with increasing chain length would be expected to decrease electron density at π*(CO) giving smaller values of Δν. Although a small difference in Δν is evident, it is smaller than expected. Broken conjugation is probably due to the known propensity of biphenyl rings to twist as in 5-Re-2 in Fig. 4 and of the phenyl rings to rotate freely as in the 5-ReP series.

Sullivan and co-workers have developed a synthetic route to linear oligomeric Re(I) polypyridine complexes by exploiting stereospecific photosubstitution of CO to give the *trans* bridged assemblies shown in Fig. 6 [66]. In the trimeric assemblies,

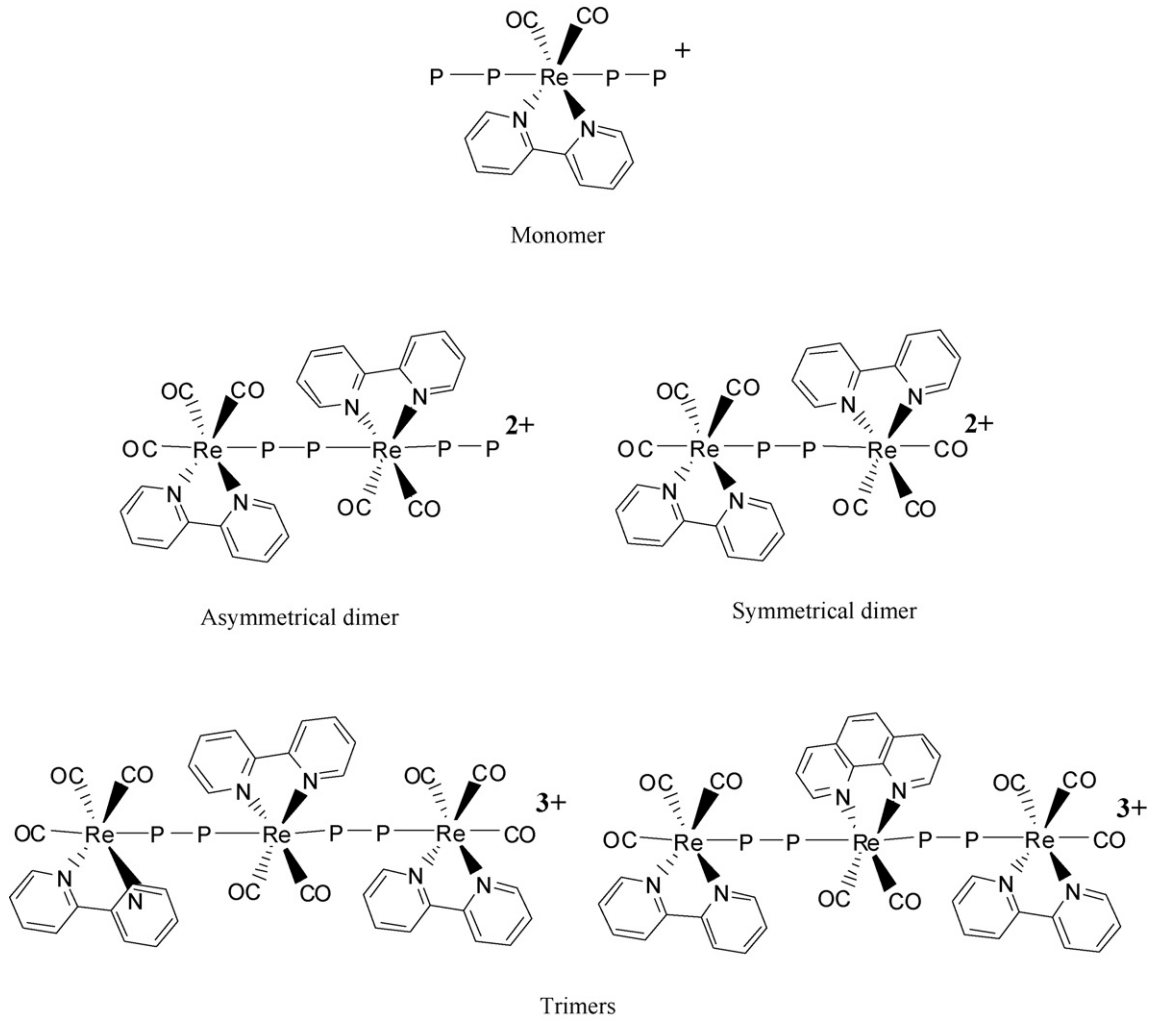

Fig. 6. Structures of phosphine-polypyridine Re complexes and assemblies. The structure of *trans*-dppene, represented by P–P, is shown in the text.

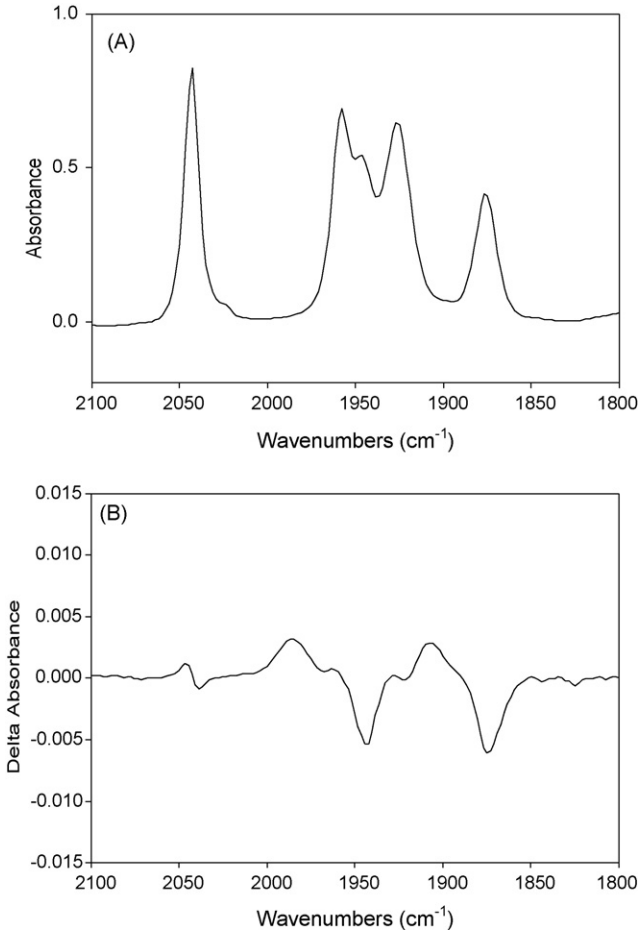

Fig. 7. Ground (A) and TRIR (B) spectra for $[(bpy)(CO)_3Re(P\text{-}P)Re(phen)(CO)_2(P\text{-}P)Re(bpy)(CO)_3(P\text{-}P)]^{3+}$ in CH_3CN at 298 K.

parallel and linear energy transfer occurred between the end units and the interior Re^I chromophore as shown by emission measurements. Representative ground- and excited-state TRIR difference spectra for $[(bpy)(CO)_3Re(P\text{-}P)Re(CO)_2(phen)(P\text{-}P)]^{2+}$ are shown in Fig. 7.

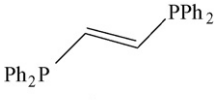

dppene

Based on steady-state emission measurements on the assemblies, efficient, rapid ($\tau < 10$ ns) excitation energy transfer occurs from the capping $[Re(bpy)(CO)_3(P\text{-}P)]^+$ units to the central chromophore $[Re(bpy)(CO)_2(P\text{-}P)_2]^+$ [66]. Efficient end-to-interior energy transfer also occurs in the extended assemblies $[(bpy)(CO)_3Re(P\text{-}P)Re(bpy)(CO)_2(P\text{-}P)Re(bpy)(CO)_3]^{3+}$ and $[(bpy)(CO)_3Re(P\text{-}P)Re(phen)(CO)_2(P\text{-}P)Re(bpy)(CO)_3]^{3+}$.

The presence of both terminal *fac*-$Re(CO)_3$ and bridging *cis*-$Re(CO)_2$ units allowed TRIR to be used to determine the equilibrated (nanosecond timescale) site of excited-state localization following laser excitation. In TRIR spectra of $[(bpy)(CO)_3Re(P\text{-}P)Re(bpy)(CO)_2(P\text{-}P)]^{2+}$, $[(bpy)(CO)_3Re(P\text{-}P)Re(bpy)(CO)_2(P\text{-}P)Re(bpy)(CO)_3]^{3+}$, and $[(bpy)(CO)_3Re(P\text{-}P)Re(phen)(CO)_2(P\text{-}P)Re(bpy)(CO)_3]^{3+}$ only *two* ν(CO) bands bleach and shift to higher energy consistent with localization of the MLCT excited states at *cis*-$Re(CO)_2$. A summary of band energies and shifts is given in Table 4 [67].

TRIR has also been applied to complexes used as building blocks for supramolecular assemblies [33,50,68]. TRIR studies have been invaluable in characterizing the excited states of chromophores containing an infrared reporter group which is sensitive to the electron density at the metal center. In a recent study TRIR was applied to the excited states of $[Ru(diimine)(CN)_4]^{2-}$ in multinuclear assemblies [68]. The $[Ru(L^2)(CN)_4]^{2-}$ ($L^2 = 2,2':3',2'':6'',2''$-quaterpyridine) core was monitored by using TRIR. The lowest-energy, excited state lifetime derived from TRIR results agreed with luminescence lifetime measurements. In more recent work these studies have been extended to a range of $[(diimine)Ru(CN)_4]^{2-}$ complexes [69].

TRIR has also been applied to the excited states of Pt(II) diimine complexes used in supramolecular assemblies, in particular, for the study of long-range energy transfer in conjugated acetylenes. In an early example, the technique was applied to the excited states of a series of $Pt^{II}(bpy)(arylacetylide)_2$ complexes [70]. In the TRIR difference spectra, Pt-to-bpy MLCT excitation induces a +25 to +35 cm^{-1} shift in ν(C≡C), the carbon–carbon triple bond stretching mode.

Picosecond TRIR has been applied to the excited states of $Pt(4,4'\text{-}(CO_2Et)_2\text{-}2,2'\text{-}bpy)Cl_2$. The lowest, short-lived excited state with $\tau = 8.7$ ps was assigned a MLCT origin based on $\Delta\nu$(C=O) ligand shifts to lower energy [32].

TRIR has also been applied to metal clusters [58,71–73] an example being an investigation of the influence of bridging CO ligands on the photochemistry of $[Ru_3(CO)_8(\mu\text{-}CO)_2(\alpha\text{-diimine})]$ (α-diimine = 2,2′-bipyridine, 4,4′-dimethyl-2,2′-bipyridine and 2,2′-bipyrimidine) [72]. These studies revealed a lowest excited state of $\pi(Ru(\mu\text{-}CO)\pi^*(\alpha\text{-diimine}))$ character. A broad transient absorption band due to bridging carbonyls is shifted to higher frequency by 35 cm^{-1} compared to the ground state. The results of related studies have been reported on the methyl-viologen-substituted cluster ($[Os_3(CO)_{10}(^iPr\text{-}AcPy)]$) [73]. TRIR results on the picosecond time showed that excitation in coordinating solvents triggers ultra-fast electron transfer from the cluster core to the remote viologen. Based on their results, electron transfer and concomitant structural change following excitation can be controlled by the redox state of the attached viologen.

The *facial* coordination geometry in complexes of the type *fac*-$[Re(L)_2(CO)_3Cl]$, with L a bridging ligand such as 4,4′-bipyridine, provides a structural basis for ligand-bridged, "molecular squares". These assemblies are of interest because of their nanometer-sized interior cavities. TRIR, in conjunction with time-resolved emission, has been used to investigate the excited-state properties of $[Re_4^I(4,4'\text{-}bpy)_4(CO)_{12}Cl_4]$ which is a member of this series [74]. The lowest ^{3}MLCT state is localized on a single Re center and one of its adjacent bridging ligands. Localization was suggested by the magnitudes of $\Delta\nu$(CO) shifts by comparison with related monomers.

Table 4
Summary of TRIR results for the series of Re MLCT oligomers shown in Fig. 6 at 298 K in CH_3CN. $\bar{\nu}_{gs}$, $\bar{\nu}_{es}$, and $\Delta\bar{\nu}(=\bar{\nu}_{es}-\bar{\nu}_{gs})$ are the ground, excited state, and excited-to-ground state $\Delta\nu$(CO) shifts and λ_{em} the CW emission maximum

Complex[a]	$\bar{\nu}_{gs}$ (cm^{-1})	$\bar{\nu}_{es}$ (cm^{-1})	$\Delta\bar{\nu}$ (cm^{-1})	λ_{em} (nm)
$[Re(bpy)(CO)_2(P\text{-}P)_2]^+$	1940	1990	+50	637
	1870	1905	+35	
$[(bpy)(CO)_3Re(P\text{-}P)Re(bpy)(CO)_2(P\text{-}P)_2]^{2+}$	2042	–	–	623
	1957	–	–	
	1942	1995	+53	
	1926	–	–	
	1870	1906	+36	
$[(bpy)(CO)_3Re(P\text{-}P)Re(bpy)(CO)_3(P\text{-}P)]^{2+}$	2042	–[b]	–	524
	1960	–	–	
	1926	–	–	
$[(bpy)(CO)_3Re(P\text{-}P)Re(bpy)(CO)_2(P\text{-}P)Re(bpy)(CO)_3(P\text{-}P)]^{3+}$	2043	–	–	
	1957	–	–	
	1945	1995	+50	615
	1926	–	–	
	1874	1906	+32	
$[(bpy)(CO)_3Re(P\text{-}P)Re(phen)(CO)_2(P\text{-}P)Re(bpy)(CO)_3(P\text{-}P)]^{3+}$	2043	–	–	602
	1957	–	–	
	1947	1985	+38	
	1926	–	–	
	1875	1907	+32	

[a] As PF_6^- salts.
[b] Unstable under the conditions of the experiment.

4.4. Competing excited-state dynamics

Assemblies have been designed in which molecular excitation is followed by two or more competitive intramolecular events. TRIR has proven invaluable in probing such competitions because of the sensitivity of reporter vibrations to differences in electronic structure. An example cited above was application of TRIR to *fac*-$[Re^I(dppz)(CO)_3(py\text{-}PTZ)]^+$ to distinguish between RS and $\pi\pi^*$ states and to monitor excited-state dynamics [29,30].

Picosecond TRIR with 400 nm excitation was applied to *fac*-$[Re(bopy)_2(CO)_3Cl]$ (bopy is 4-benzoylpyridine) revealing a $\Delta\nu$(CO) shift of $+54\,cm^{-1}$ for the A′(1) mode and $\Delta\nu(C{=}O) = -55\,cm^{-1}$ for the ketone [75]. The directions of the shifts were consistent with a lowest-lying $d\pi(Re)\text{-}\pi^*(bopy)$, MLCT excited state.

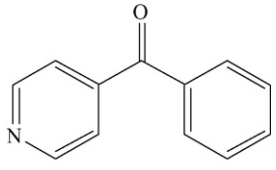

bopy

However, the $\Delta\nu$(CO) shift for A′(1) is significantly larger than in the MLCT excited states of $[Re(dmb)(CO)_3(Etpy)]^{+*}$ or *fac*-$[Re(bpy)(CO)_3(bopy)]^+$ and there was no observable shift in ν(C=O) for the ketone. These and complementary TR^3 results are consistent with a lowest MLCT state with bopy as the acceptor ligand with extensive charge localization. On the picosecond timescale both instantaneous and temporally evolving ν(CO) components are observed for the MLCT excited states of both *fac*-$[Re(bopy)_2(CO)_3Cl]$ and *fac*-$[Re(bpy)(CO)_3(bopy)]^+$. These excited states are formed vibrationally hot and evolve quickly after excitation.

Complexes of the type *trans*,*cis*-$[M(\alpha\text{-diimine})(CO)_2(SnR_3)_2]$ ((α-diimine=bpy) M = Ru, Os; R = Ph, Me) are also known to undergo complex excited state dynamics following excitation [50]. The lowest energy electronic transition is sigma-bond-to-ligand charge transfer (SBLCT), $\sigma(Sn-M-Sn)\xrightarrow{h\nu}\pi^*(\alpha,\alpha\text{-diimine})$. Consistent with this assignment, low energy excitation induces $M{-}SnR_3$ bond breaking. Bond breaking is inhibited in low temperature glasses where translational mobility is low.

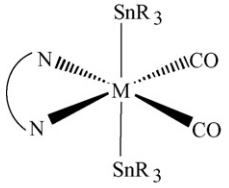

M = Ru, Os
R = Me, Ph

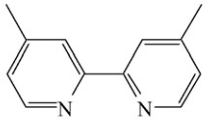

dmb

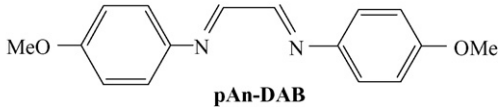

pAn-DAB

Variations in the diimine ligand were used to vary the π^* level in the series: pAn-DAB < iPr-DAB < dmb. In the ground

state, this led to a slight decrease in $\bar{\nu}$(CO) across the series as the metal became more electron rich. Comparison of the ν(CO) band positions shows that replacement of $SnMe_3$ by $SnPh_3$ causes a shift of the CO-stretching vibrations to higher energy. In $[Ru(SnR_3)_2(CO)_2(dmb)]$, ν(CO) bands for R = Me appear at lower energy by 12 and 14 cm^{-1} compared with R = Ph. Excited state TRIR spectra for all complexes were obtained in frozen butyronitrile:propionitrile glasses, and for $[Os(dmb)(CO)_2)(SnR_3)_2]$, in a frozen BuCN-PrCN solution at 77 K. For the dmb complexes $\Delta\nu$(CO) shifts were small and positive in all cases with substitution by DAB causing no or slightly negative shifts. DFT calculations aided in the interpretation of the results and pointed to significantly decreased excited state charge transfer character upon substitution of dmb for DAB.

4.5. Isomerization

TRIR has also been invaluable in studying intramolecular sensitization of ligand isomerization. These processes are of interest because sensitized photoisomerization of coordinated ligands can lead to rapid (sub-nanosecond), sensitive, and even dramatic light on/off effects which are of potential interest in photochromic materials.

4.5.1. Trans-cis isomerization in olefins

Photoisomerization in stilbenes is well known and studied [76–82]. In fact, as a class, the stilbenes are considered to be the "model" for understanding olefin isomerization mechanisms. The triplet manifold including the lowest $^3\pi\pi^*$ and twisted triplet (perpendicular) states, $^3p^*$ (^3IL_p), can be accessed by heavy atom effects or by inter- or intramolecular energy transfer.

In *fac*-$[Re(phen)(CO)_3(bpe)]^+$ (bpe is 1,2-bis(4-pyridyl) ethylene), the absorption spectrum is dominated by intraligand $\pi \rightarrow \pi^*$ and Re → phen, bpe transitions between 310 and 370 nm.

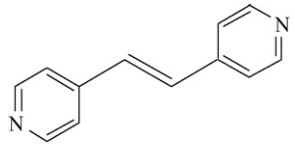

bpe

Excitation in this spectroscopic range results in isomerization at the bpe ligand in solution, Eq. (3). Isomerization is inhibited in a 1:1 propionitrile:butyronitrile glass at 77 K.

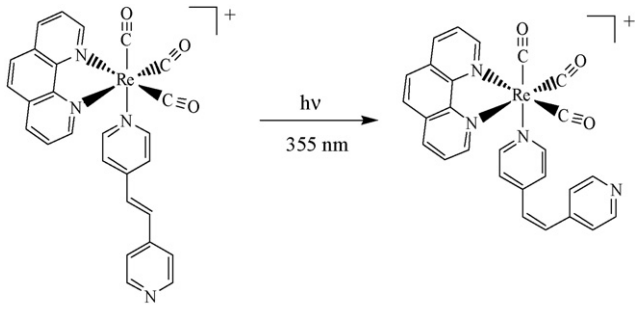

fac-$[Re^I(phen)(CO)_3(trans\text{-}bpe)]^+$ *fac*-$[Re^I(phen)(CO)_3(cis\text{-}bpe)]^+$ (3)

TRIR measurements, combined with CW emission and transient absorption measurements, were used to gain insight into the mechanism of isomerization [83]. In the ground state ν(CO) spectrum in acetonitrile, the A_1 and E bands of *fac*-$Re(CO)_3$ appear at 1934 and 2035 cm^{-1}. Following laser flash excitation at 355 nm, a short-lived intermediate ($\tau \sim 28$ ns) appears with $\bar{\nu}$(CO) at 1927 and 2029 cm^{-1} ($\Delta\bar{\nu}$(CO) = −6 and − 7 cm^{-1}). The negative shifts suggest a lowest bpe-localized excited state, either a triplet, $^3t^*(^3IL_t)$, or the twisted triplet, $^3p^*(^3ILp)$. In an extension of the TRIR scan to 1100 cm^{-1}, ν(C=C) shifts to lower energy were observed from 1639 to 1622 cm^{-1} consistent with significant charge redistribution at the ligand and a twisting around the double bond.

Continued photolysis of *fac*-$[Re(phen)(CO)_3(trans\text{-}bpe)]^+$ produces the *cis*-photoproduct. At room temperature in solution it has a reversed excited state ordering with $^3MLCT < ^3c^*(^3IL_c)$. Appearance of the *cis*-product was accompanied by an MLCT-based emission at 550 nm with $\tau \sim 928$ ns. As shown in the TRIR spectrum of a pre-photolyzed mixture (64% *cis*/36% *trans*) both *positive* and *negative* $\Delta\bar{\nu}$(CO) shifts appear consistent with the simultaneous presence of both MLCT and $^3c^*$ excited states.

TRIR was also applied to ligand isomerization in the related styrylpyridine-containing complexes *fac*-[Re(*trans*-4-styrylpyridine)$_2$$(CO)_3Cl]^+$ and *fac*-$[Re(bpy)(CO)_3$(*trans*-4-styrylpyridine)$]^+$ [84]. MLCT excitation in these complexes is followed by rapid intramolecular energy transfer to a triplet intraligand state localized on the styrylpyridine (stypy) ligand, ^3IL.

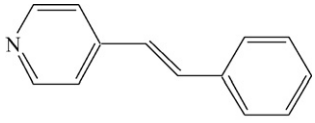

(4-styrylpyridine)

Following excitation of *fac*-[Re(*trans*-4-styrylpyridine)$_2$ $(CO)_3Cl]^+$ at 400 nm, $\Delta\bar{\nu}$(CO) values are slightly negative, consistent with a lowest stypy-based $\pi\pi^*$ excited state. The spectrum evolves over 40 ps. Busby and co-worker propose the intervention of two ^3IL states with initial formation of ^3IL_t, the triplet *trans* intraligand $\pi\pi^*$ state, followed by rapid evolution to ^3IL_p, the twisted ligand-based state. The latter is observed from ∼70 ps to 1 ns.

Support for the twisted state comes from measurements in the olefin ν(C=C) stretching region in the rigid medium poly(methylmethacrylate) (PMMA). In this medium rotation around the olefin and conversion of ^3IL_t to ^3IL_p is hindered and there is no spectroscopic evolution in the ν(CO) region on the 40–70 ps timescale.

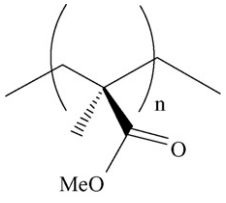

(PMMA)

For *fac*-$[Re(bpy)(CO)_3$(*trans*-4-styrylpyridine)$]^+$ in solution, the characteristic large, positive $\Delta\nu$(CO) shifts of an initially

formed ^{3}MLCT state are observed but disappear within 6–10 ps [84]. An IL state is formed concomitantly with slightly negative $\Delta\nu$(CO) shifts that were also assigned to a twisted triplet state on styrylpyridine, ^{3}ILp.

In the naphthyl derivative, 1-(1-hydroxy-2-naphthyl)-3-(1-naphthyl)-2-propen-1-one), Kaneda and co-workers probed *trans*- to *cis*-isomerization by monitoring the ν(C=C) stretch following excitation in CCl_4 [85]. A bleach was observed corresponding to ν(C=C) at 1576 cm^{-1} with a negative shift (to 1500 cm^{-1}) of a weak absorption feature that could be assigned to either (*cis*- or *trans*-) keto tautomer. The bleach recovered within 2 ms.

4.5.2. Other forms of isomerization

TRIR has found general use in elucidating photo-isomerization mechanisms in transition metal complexes. One example is in linkage or coordination isomerization in which a bound ligand undergoes a change in the nature of its coordination following excitation. An example occurs in the series M(CO)$_5$(DHF) (M = Cr, Mo, W; DHF is 2,3- or 2,5-dihydrofuran) [86].

Photolysis of M(CO)$_5$(cyclohexane) in the presence of DHF gives M(CO)$_5$($^1\eta$-DHF) with DHF bound via the oxygen atom of the DHF ring. At longer photolysis periods, an equilibrium develops between $^1\eta$- and $^2\eta$-isomers. In the latter, the ligand is bound through the C=C double bond of the ring. TRIR in the ν(CO) region on the millisecond timescale was used to monitor the kinetics of linkage isomerization with rate constants and activation parameters determined as a function of metal. In complexes, independent of metal, the initial product was M(CO)$_5$($^1\eta$-DHF). This kinetic product undergoes isomerization to give a mixture of $^1\eta$- and $^2\eta$-isomers. In the W analog (but not for Mo or Cr) isomerization was also found to occur at a faster rate for the 2,3-DHF ($\sim$1000 s^{-1}) complex compared to 2,5-DHF (4 s^{-1}). Activation energies for isomerization were on the order of 10–15 kcal mol^{-1} with the order of decreasing isomerization rate: Mo > Cr > W. It was also possible to predict trends in equilibrium parameters from the experimental results based on hard/soft and electronic structure arguments. The "softer" metal, W, shows a preference for the $^2\eta$ form, and for coordination of softer ligands.

In an earlier report, arene ring isomerization in η^6-arene metal carbonyl complexes such as [Cr(η^6-2,6-X$_2$C$_5$H$_5$N)(CO)$_3$] (X = H or (CH$_3$)$_3$Si (IMS)) was reported [87]. Photochemical arene exchange had been previously reported to occur via a carbonyl-loss intermediate and the π-bonded pyridines offered multiple coordination motifs through the π system or directly through the nitrogen. Photolysis of this complex in CO-saturated acetonitrile, methanol, or cyclohexane solutions monitored by UV/vis measurements showed loss of absorbances characteristic of the parent complex and formation of bands associated with [Cr(η^6-C$_5$H$_5$N)(CO)$_3$]. Isolation of the parent complex in a solid methane matrix at 10 K did not inhibit ligand-loss photochemistry. The loss of absorption of the CO bands at 1999, 1938, and 1924 cm^{-1} occurred concomitantly with formation of bands at 1957, 1841, and 1833 cm^{-1}. These observations were consistent with the facial tri-carbonyl, heteroarene ring-slip product [Cr(η^x-C$_5$H$_5$N)(CO)$_3$] ($x < 6$).

By doping the methane matrix with N_2 and CO, the authors were able to "tune" the hapticity of the pyridine ligand by coordination with the dopant molecules, e.g. to form [Cr(η^x-C$_5$H$_5$N)(CO)$_3$(N$_2$)$_2$] ($x = 1$), and [Cr(η^x-C$_5$H$_5$N)(CO)$_2$(N$_2$)$_2$] ($x = 6$) in the case of N_2 doping. Similar behavior was observed with added CO. Surprisingly, photolysis of the TMS-substituted parent complex at 460 nm in an Ar matrix with added CO did not produce IR spectroscopic changes. Shifting the photolysis wavelength to 250 nm revealed a disappearance of absorbances due to the parent complex, and the growth of bands at energies corresponding to the bis-carbonyl [Cr(η^6-2,6-X$_2$C$_5$H$_5$N)(CO)$_2$] (X = (CH$_3$)$_3$Si). Additional photolysis resulted in tricarbonyl formation and η^1 ring coordination.

TRIR measurements on [Cr(η^6-C$_5$H$_5$N)(CO)$_3$] in CO-saturated cyclohexane revealed bleaches at 1999, 1940, and 1930 cm^{-1} and the growth of bands at 1950, and 1890 cm^{-1}. Inspection of the transient data revealed formation of both the bis-carbonyl [Cr(η^6-C$_5$H$_5$N) (CO)$_2$(Sol)] and the η^1 pentacarbonyl. The transient results were essential in revealing that CO ligand loss is not the only photochemical reaction pathway available. However, it was the use of multiple techniques, including TRIR, that shed light on the multiplicity of available photochemical pathways. The formation of the high carbonyl-count intermediates depends not only on the solvent environment, but also substitution of the pyridine ring which causes steric crowding of the coordination environment.

4.6. Complex excited states: case studies

Transition metal complexes containing flat planar aromatic ligands such as dppz (dppz = dipyrido[3,2-a:2′,3′-c]phenazine) have been used as probes to study DNA mediated electron transfer and DNA damage because they intercalate into the DNA double helix forming a molecular "light switch" [88]. Dppz-containing complexes of Ru(II), Os(II) and Re(I) have been extensively studied in this regard by time-resolved and steady state spectroscopic techniques.

Electronic complexity exists in these excited states arising from nearly localized phenanthroline-like and phenazine-like π^* acceptor levels. The close proximity of these levels leads to closely lying $\pi\pi^*$, IL, and MLCT states based on separate phenanthroline and phenazine fragments. The relative energies of the two kinds of levels can be changed by varying substituents on the ligand or solvent including H-bonding.

In CO-containing complexes, ν(CO) bands and TRIR have been applied to differentiating among MLCT, IL, and $\pi\pi^*$ excited states and whether they are localized on the phen or phenazine fragments. The combined results of picosecond and nanosecond TRIR, transient absorption, and TR^3 measurements have been used to demonstrate that photoexcitation of *fac*-[Re(dppz)(CO)$_3$(py)]$^+$ results in a thermally relaxed ^{3}IL $\pi\pi^*$(dppz) state on the ns timescale. This state is formed within 30 ps from a precursor state, is emissive, and equilibrates with a close-lying ^{3}MLCT excited state on the nanosecond timescale [35]. Two bands corresponding to the carbonyl modes are found at 2036 and 1933 cm^{-1}. At short times following excitation (1 ps), the two ground-state bands bleach and bands associ-

ated with the excited state are found shifted to lower energies at 2016 and 1907 cm^{-1}. The shifts to lower energy are consistent with an intraligand state, localized on dppz, a poor π-acceptor in the excited state. As the probe delay is increased, the two bands related to the excited state narrow and shift slightly (by ~7 cm^{-1}) to higher energy. The evolution of ν(CO) is related to the evolution of the ^{3}IL (^{3}ππ*(dppz)) state from a largely phen-localized state to a largely phenazine (phz)-localized state. The evolution of the intraligand state moves electron density farther away from Re, decreasing dπ(Re)–π*(CO) backbonding even more than in the initially formed (1 ps) state.

A TRIR study on [Re(dppz-Cl_2)(CO)$_3$(L)]$^{n+}$ (L = Cl^- (n = 0), py (n = 1) and (4-dimethylamino)pyridine (n = 1)) in CH_3CN at room temperature illustrated the power of the technique to unravel competing excited-state processes in dppz complexes [89]. While *fac*-[Re(dppz-Cl_2)(CO)$_3$Cl] does not emit at room temperature [90], *fac*-[Re(dppz-Cl_2)(CO)$_3$(py)]$^+$ does and with the clearly resolved vibrational structure characteristic of an IL state. The relatively short excited-state lifetime, τ = 7 ns, suggested an additional complication in the excited-state manifold. Emission from *fac*-[Re(dppz-Cl_2)(CO)$_3$(4-Me_2Npy)]$^+$ at 570 nm is broad and featureless and decays with τ = 1.5 (±1) ns.

In the TRIR spectrum of *fac*-[Re(dppz-Cl_2)(CO)$_3$(py)]$^+$ in CH_3CN obtained following excitation at 400 nm, there was only evidence for a IL ππ* excited state. With L = 4-Me_2Npy two sets of ν(CO) bands were observed arising from IL ππ* and Re-phenazine MLCT states. In the TRIR spectrum of *fac*-[Re(dppz-Cl_2)(CO)$_3$Cl], there was evidence for only a phenazine-localized MLCT state. The photophysics of these complexes has been examined in subsequent papers [34].

4.7. Medium effects

4.7.1. Medium as an energy gap effect

The solvent can play a significant role in charge transfer processes [91]. The solvent influences the transition between states in two ways. One is through ΔG and differences in solvation energies. The other is through its contribution to the reorganization energy arising from changes in solvent dipole interactions with the ligands and their associated charge distributions in initial and final states. The classical reorganization energy associated with electron transfer reactions, and charge transfer in general, can be partitioned into intramolecular (λ_i) and solvent (λ_o) terms, $\lambda = \lambda_i + \lambda_o$ [91–97].

Following Marcus, the solvent, or medium, reorganization energy can be further divided into frozen, λ_{oo}, and unfrozen, λ_{io}, parts with $\lambda_o = \lambda_{oo} + \lambda_{io}$ [96–98]. In the classical, dielectric continuum limit, the magnitude of λ_{oo} depends on both excited-state and ground-state vector dipole moments ($\vec{\mu}_f$, $\vec{\mu}_i$) and the optical and static dielectric constants of the medium. For charge transfer excited states in rigid media, λ_{oo} becomes part of ΔG as shown for the free energy of an excited state in a frozen (fr) medium, ΔG_{ES}, compared to a comparable fluid (fl), Eq. (4).

$$\Delta G_{ES}(\text{fr}) \sim \Delta G_{ES}(\text{fl}) + \lambda_{oo} \quad (4)$$

A blue-shifted emission is observed for MLCT excited states in frozen media compared to solution, a phenomenon that has been termed "rigidochromism" [99–109]. The origin of the effect is included in Eq. (4). For a Gaussian shaped band in the classical limit, $\bar{\nu}_{em} = \Delta G^0_{ES} - \lambda_i - \lambda_o$, while in a rigid medium, $\bar{\nu}_{em} = (\Delta G^0_{ES} + \lambda_{oo}) - \lambda_i - \lambda_{o,i}$. For ligand-localized ππ* excited states, interaction with the solvent is much less and emission energies are relatively unaffected by the transition from fluid to glass [91,102].

Related effects are observed by TRIR for ν(CO) in rigid media [110]. In a study by Clark et al., it was reported that the magnitudes of Δν(CO) shifts in the MLCT excited state of *fac*-[Re^I(bpy)(CO)$_3$Cl] are less in a frozen nitrile glass at 77 K than in fluid solution [110]. This was attributed to an increase in excited-state energy in the rigid medium which enhanced MLCT excited-state mixing with low-lying ππ*(bpy) excited states. In related Re complexes, ligand-localized and MLCT excited states are known to lie close in energy with the state ordering depending on the ligands, the medium, and the temperature [34,91,99,111–125].

The carbonyl shifts in the excited state of [Os(dmb)(CO)$_2$($SnPh_3$)$_2$] were compared both at 77 K in a frozen BuCN-PrCN (5:4 v/v) glass and at room temperature in the fluid. Nanosecond TRIR measurements revealed that both ν(CO) bands shift to higher energy, but by +14 cm^{-1} in solution compared to +10 cm^{-1} in the glass. The difference in shifts between the two media was attributed to incomplete charge transfer after excitation due to the lack of dipole reorganization of the solvent.

Dattelbaum and Meyer reported TRIR results on the series, *fac*-[Re^I(4,4′-X_2bpy)(CO)$_3$(4-Etpy)]$^+$ (X = CH_3, H, CO_2Et) at room temperature in poly-methylmethacrylate (PMMA) films [26]. Film TRIR spectra were qualitatively similar to solution spectra, with the two ground state ν(CO) bands splitting into three in the excited state.

Ground state band energies were relatively unaffected by the choice of medium, but smaller Δν(CO) shifts were observed for the excited states in PMMA even though the energy gap, E_0, was increased. A plot of excited-state vibrational frequencies $\bar{\nu}_{es}$(CO) versus ground-to-excited state energy gap (E_0) is shown in Fig. 8. The energy gap was determined by independent emission measurements and emission spectroscopic fitting for the complexes in both solution and PMMA films. The smaller shifts in PMMA were attributed to the increase in the ground-to-excited state energy gap, E_0, in this series, which is principally related to increasing the energies of the π*(4,4′-X_2bpy$^{\bullet-}$) levels. This, in turn, increases π*(4,4′-X_2bpy$^{\bullet-}$)-π*(CO) orbital mixing which causes the decreased Δν(CO) shifts in PMMA with increasing energy gap, E_0. A related trend was noted in solution with $\bar{\nu}_{es}$(CO) decreasing in the series *fac*-[Re(4,4′-X_2bpy)(CO)$_3$(4-Etpy)]$^+$ as the energy gap was increased. The influence of substituent -X is similar to that of the medium, and trends in $\bar{\nu}_{es}$(CO) arise from the influence of -X on the lowest π* acceptor level [110].

An important conclusion is that $\bar{\nu}_{es}$(CO) varies with E_0 *regardless of whether -X or the medium is varied*. E_0 is the fundamental parameter. Linear correlations were found between

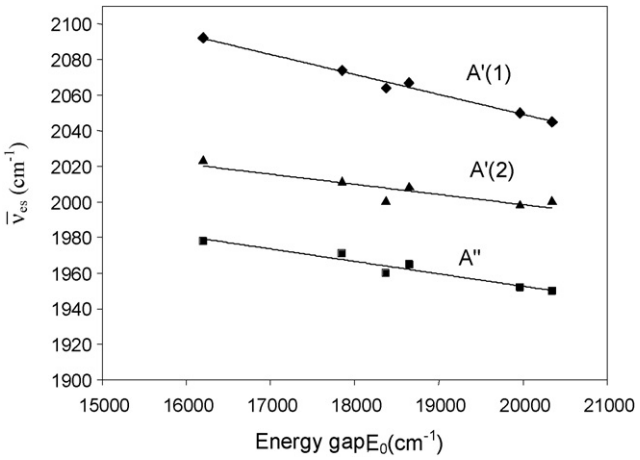

Fig. 8. Plots of excited state vibrational frequency ($\bar{\nu}_{es}$) vs. ground-to-excited state "energy gap" E_0 for *fac*-[Re^{I}(4,4′-X$_2$bpy)(CO)$_3$(4-Etpy)]$^+$ in CH_3CN and PMMA for the A′(1) (♦), A″ (■), and A′ (2) (▲) normal modes [26].

$\bar{\nu}_{es}$(CO) and E_0 for all three carbonyl modes, Fig. 8, with $\bar{\nu}_{es}$(CO) decreasing as E_0 increases.

These observations point to a common orbital origin for medium and substituent effects based on π^*(4,4′-X$_2$bpy$^{\bullet-}$)-π^* (CO) orbital mixing. With this interpretation, the IR ν(CO) MLCT rigidochromism effect is a consequence of MLCT (dπ(Re)-π^*(CO))-MLCT (dπ(Re)-π^*(4,4′-X$_2$bpy)) excited state mixing and not due to MLCT-$\pi\pi^*$ excited state mixing.

Smith and co-workers performed TRIR measurements on the nanosecond timescale on Pt(II) and Ru(II) complexes embedded in KBr pellets [126]. The use of KBr is particularly interesting because it is transparent over the entire mid-infrared region. TRIR spectra of [Ru(bpy)$_2$(4-COOEt-4′-CH$_3$bpy)]$^{2+}$ in KBr and acetonitrile solution were compared. The ester ν(C=O) mode of the substituted bipyridine ligand shifts to lower energy upon photoexcitation consistent with a substituted-bpy-localized MLCT excited state, regardless of media. The magnitude of the shift was comparable in the two media, and despite exposure to air, there was no appreciable O_2 quenching of the excited state(s) in the KBr pellet. The technique was also applied to the insoluble Pt(II) complex, [Pt(dpphen)(dcbdt)] (dpphen is 4,7-diphenyl-1,10-phenanthroline, dcbdt is *N*,*N*′-dicyclohexyl-(1,1-dithiolatomethylene)barbituric acid) [126].

Rigid media have also been found to stabilize complexes that are photochemically unstable in solution, especially toward ligand loss due to low lying dd (Ligand Centered) excited states. For Ru(II) polypyridine complexes, these states are typically populated following MLCT excitation and MLCT → dd surface crossing [127–139].

It is possible to avoid dd states in Ru(II) complexes by appropriate ligand variations which increase the dd-MLCT energy gap [130,135,140]. Another strategy is the use of rigid (solid) matrices, such as poly(methyl methacrylate), or low temperature glasses, to stabilize metal complexes toward ligand loss [7]. The use of this strategy coupled with transient near IR (TRNIR) measurements to investigate the excited-state mixed valence properties of *cis*,*cis*-[(bpy)$_2$ClRu(pz)RuCl(bpy)$_2$](PF$_6$)$_2$ is discussed in Section 5.

4.7.2. Surfaces

Recently, time resolved step-scan FT-IR spectroscopy has been adapted to imaging by using a step-scan FT-IR instrument coupled to an IR microscope giving 3 μm spatial resolution on the microsecond timescale [141,142]. In this study, imaging-TRIR was applied to polymer-dispersed liquid crystal (PDLC) E7 in a thiolene polymer matrix on conductive indium tin oxide-coated CaF_2 plates. An electric field applied to the PDLC was used to induce rotational reorganization of the molecules. The molecular dipole vector aligns with the field causing a bleach or decrease in the transient absorption signal. In Fig. 9 is shown the temporal response of ν(CN) of the liquid-crystal at 2227 cm^{-1} following the applied electric field. The liquid crystal aligns with the applied field rapidly, as shown by the bleaching of the nitrile band in the TRIR images. The molecule then slowly reorients back to its original conformation over several hundred milliseconds.

The medium can also be an active participant in excited-state processes either participating in electron transfer or coordinating to a photoactive intermediate. A rigid medium or interface can also act as an active electron acceptor, as is commonly observed in nanocrystalline semi-conductor materials such as TiO_2. d^6 transition metal chromophores covalently linked to semiconductor surfaces provide the basis for some of the most efficient photovoltaic materials. Understanding electron transfer efficiencies and dynamics at and between the coupled complex-semiconductor interface is a key to the design of more efficient solar devices.

Interest in these "dye-sensitized" photovoltaics has led to extensive study of excited state electron injection into TiO_2. Heimer and Heilweil monitored electron injection into TiO_2 by surface-bound, excited [Ru(4,4′-(COOCH$_2$CH$_3$)$_2$-2,2′-bipyridine)(2,2′-bipyridine)$_2$]$^{2+}$ by monitoring ν(C=O) shifts of the bound ligand with picosecond pump-probe broadband transient infrared spectroscopy [143]. Based on their data, they were able to assign a lower limit for the rate constant for electron injection of 5.0×10^{10} s^{-1}.

Mid-infrared transient absorption spectroscopy has also been used to monitor the injected electrons with step-scan TRIR used to measure slower (ns) processes such as back electron transfer recombination at the interface. Faster methods have been used to study the electron injection process directly [144,145]. Lian and co-workers have studied electron injection by the commonly used solar cell dyad of Ru N3, [Ru(dcbpy)$_2$(NCS)$_2$] (dcbpy = 4,4′-dicarboxy-2,2′-bipyridine), bound to TiO_2 [144,146,147]. A maximized incident-photon-to-current-efficiency (IPCE) for this arrangement of >80% has been reported [148,149]. Dye sensitized TiO_2 films exhibit a broad transient absorption feature between 2 and 7 μm attributed to injected electrons. Control experiments with the Ru N3 dye on Al_2O_3 (in which the conduction band is too high for electron injection) show no related feature, likewise for bare TiO_2. Injection is characterized by both fast and slow components, with the fast component occurring in ∼50 ± 25 fs, and the slow compo-

nent occurring at ~2 ps. The slow component has been shown to be highly sensitive to the age of the film itself. Injection rates are similar for a variety of surface-bound sensitizers, all having times of <100 fs.

Lian and co-workers have also extended this work to examine a series of dyes on TiO_2 including $[Ru(dcbpy)_2(X)_2]^{2+}$ (dcbpy is 4,4′-dicarboxyl-2,2′-bipyridine; $(X)_2$ is $(CN^-)_2$, $(SCN^-)_2$, or dcbpy) and $Re(dcbpy)(CO)_3Cl$ [144]. For the complexes with X = CN and SCN, the energy of the adsorbed ^{3}MLCT excited state lies above the TiO_2 conduction band edge. However, for $[Ru(dcbpy)_3]^{2+}$ it lies 200 mV below the conduction band edge. It was hypothesized that its injection rate should be substantially slower or not occur to any appreciable extent. For all three samples, the rise time for electron injection remained <100 fs but the signal intensity for injected electrons increased in the order $NCS^- > CN^-$ > dcbpy as 1.0:0.8:0.5. This suggested that interfacial electron injection must compete with intramolecular relaxation on the surface for $[Ru(dcbpy)_3]^{2+*}$.

For $[Re(dcbpy)(CO)_3Cl]$, TRIR was used to monitor $\Delta\nu$(CO) coincident with electron injection and oxidation of the complex [150]. A bleach in the band for the A′(1) mode at 2047 cm^{-1} with a concomitant ground-to-excited state shift of +23 cm^{-1} (to 2070 cm^{-1}) was observed. No further growth of oxidized dye was observed after the first 200 fs. The broad IR signal associated with injected electrons maximized in less than 100 fs similar to the Ru complexes. For the Re complex it was suggested that electron injection occurs prior to vibrational relaxation since the energy of the equilibrated ^{3}MLCT state is below the conduction band edge. Vibrational cooling in the ν(CO) modes was observed between 0.2 and 10 ps with a blue shift from 2060 to 2070 cm^{-1}.

Lian and co-workers have extended the application of TRIR to study electron injection as a function of the semiconductor, SnO_2 and ZnO [151], adsorbed dye (for example, to Coumarin 343 and $Fe(CN)_6^{4-}$ [152,153], distance from the surface by varying the linker [154], trap sites [155], and pH [156]. Electron injection rise times in SnO_2 and ZnO were much slower (3.2 and 100 ps, respectively) than in TiO_2 and multi-exponential.

5. Spectroscopic extension into the near-IR

Nanosecond step-scan FT-IR measurements have been extended into the near-infrared (time-resolved near-infrared spectroscopy (TRNIR)) which allows for measurement of low energy electronic absorption bands in molecules and semiconductors and vibrational overtones. Application to dye-sensitized photoinjection in semiconductors was already mentioned in Section 4.7. The technique has been applied to the detection of $^1O_2$ in photodynamic therapy and the use of an IR microscope has allowed imaging of $^1O_2$ in living cells following laser excitation [157].

In 2002, the first observation of a transient intervalence transfer absorption band in the near IR on the nanosecond timescale was made [158]. The spectrum was obtained by modification of a Bruker IFS 66V/s instrument, allowing transient spectra to be measured to ~12,500 cm^{-1}. Laser flash, $Ru^{II} \rightarrow$ tppz excitation was used to generate a transient mixed valency in the complex $[(tpy)Ru(tppz)Ru(tpy)]^{4+}$, (tpy is 2,2′:6′,6″-terpyridine, tppz is

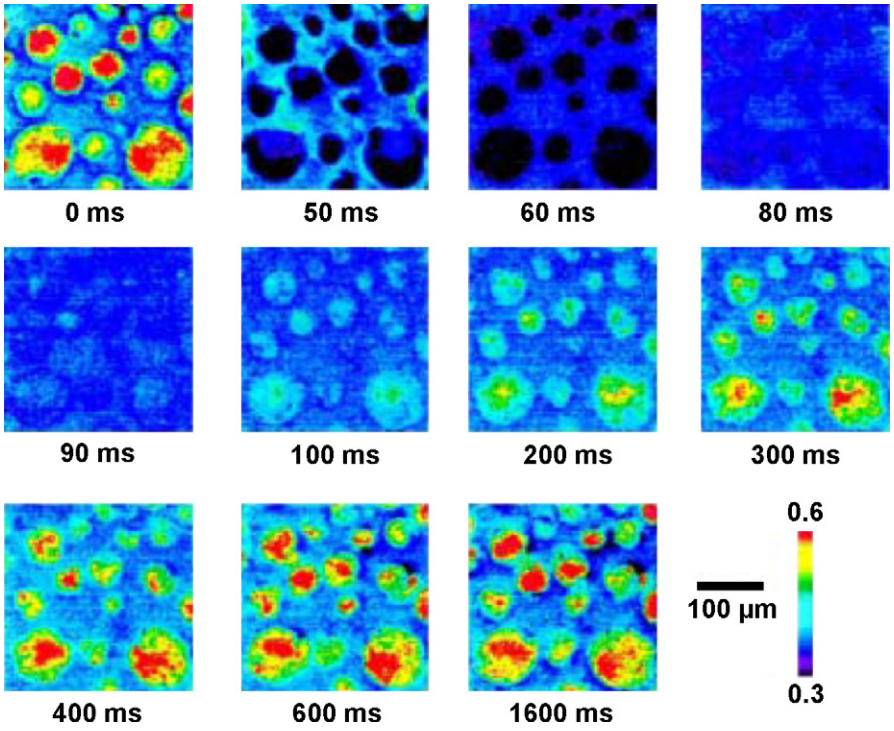

Fig. 9. Temporal response of ν(CN) at ~2227 cm^{-1} in the absorption distribution of polymer-dispersed liquid crystal (PDLC) E7 in a thiolene polymer matrix on conductive indium tin oxide-coated CaF_2 plates [157]. An electric field applied to the PDLC was used to induce rotational reorganization of the molecules followed by relaxation. The molecular dipole vector aligns with the field causing a bleach or decrease in the transient absorption.

2,3,5,6-tetrakis(2-pyridyl)pyrazine), Eq. (5).

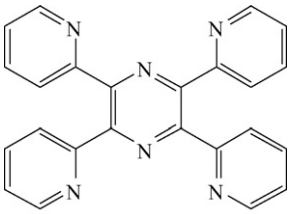

tppz

$$[(tpy)Ru^{II}(tppz)Ru^{II}(tpy)]^{4+} \xrightarrow{h\nu} [(tpy)Ru^{III}(tppz^{\bullet-})Ru^{II}(tpy)]^{4+*} \quad (5)$$

In related mixed-valence ground-states, intervalence transfer (IT) measurements have provided a powerful experimental probe for exploring the relationship between optical and thermal electron transfer, electronic delocalization, and solvent effects. Analysis of IT bands, which typically appear in the near IR, has been used to provide activation barriers and reorganization energies and, from integrated band intensities, the extent of electronic coupling [159–164]. It is an important probe since direct measurement of electron transfer, M^{II}-L-$M^{III} \rightarrow M^{III}$-L-$M^{II}$, has proven to be difficult experimentally.

The lifetime of $[(tpy)Ru(tppz)Ru(tpy)]^{4+*}$ in CH_3CN at 298 K is $\tau \sim 82$ ns which was sufficiently long to search for a possible excited-state IT band by nsec TRIR. The excited-state IT absorption, Eq. (6), is shown in Fig. 10.

$$[(tpy)Ru^{III}(tppz^{\bullet-})Ru^{II}(tpy)]^{4+*} \xrightarrow{h\nu} [(tpy)Ru^{II}(tppz^{\bullet-})Ru^{III}(tpy)]^{4+*} \quad (6)$$

The lifetime for the near-IR transient shown in the inset in Fig. 10 is consistent with the MLCT excited-state lifetime measured by emission. Based on an analysis of IT band shapes, it

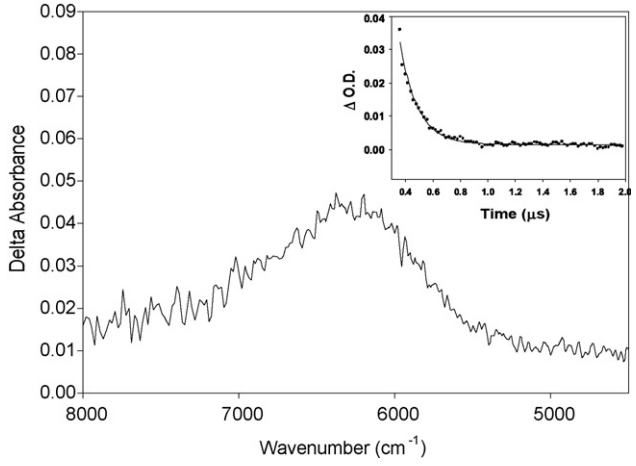

Fig. 10. Transient absorption near IR (TRNIR) difference spectrum obtained 20–40 ns after laser flash excitation (500 μJ/pulse) of $[(tpy)Ru^{II}(tppz)Ru^{II}(tpy)]^{4+}$ at 548 nm in CD_3CN at 298 K. Samples were purged with Ar prior to measurement. The inset shows a plot of exponential transient decay measured by TRNIR with $k = 7.73 \times 10^6\ s^{-1}$ ($\tau = 129 \pm$ ns) [158].

was concluded that both ground- and excited-state complexes are either in Class II-III (solvent averaged, localized oxidation states) [91] or Class III (delocalized) in the modified Robin and Day classification system. The excited-state experiment allows comparison to be made between tppz and $tppz^{\bullet-}$ as bridging ligands.

A second example, *cis*,*cis*-$[(bpy)_2ClRu(pz)RuCl(bpy)_2](PF_6)$ in PMMA films, was also investigated [29]. In solution, this complex is photochemically unstable toward ligand loss but, as noted in the previous section, photodecomposition can be minimized or even eliminated in rigid media such as PMMA.

Laser excitation at 510 nm in CD_3CN at 298 K gives the ^{3}MLCT state *cis*-,*cis*-$[(bpy)_2ClRu^{III}(pz^{\bullet-})Ru^{II}Cl(bpy)_2]^{2+*}$, Eq. (7). Its appearance is accompanied by a transient near-IR feature at $\bar{\nu}_{max} = 6880\ cm^{-1}$ with $\Delta\bar{\nu}_{1/2} = 3740\ cm^{-1}$ and $\varepsilon_{max} \geq 970\ M^{-1}\ cm^{-1}$.

$$[(bpy)_2(Cl)Ru^{II}(pz)Ru^{II}(Cl)(bpy)_2](PF_6)_2 \xrightarrow{h\nu} [(bpy)_2(Cl)Ru^{III}(pz^{\bullet-})Ru^{II}(Cl)(bpy)_2](PF_6)_2{}^* \quad (7)$$

Comparison of the excited state and related ground-state ($\bar{\nu}_{max} = 7700\ cm^{-1}$, $\Delta\bar{\nu}_{1/2} = 5000\ cm^{-1}$, $\varepsilon_{max} = 455\ M^{-1}\ cm^{-1}$ in CD_3CN at 298 K) IT bands, Eq. (8), revealed that the extent of metal–metal electronic coupling is comparable even though the orbital mechanisms for coupling are considerably different.

$$[(bpy)_2(Cl)Ru^{III}(pz^{\bullet-})Ru^{II}(Cl)(bpy)_2](PF_6)_2{}^* \xrightarrow{h\nu} [(bpy)_2(Cl)Ru^{II}(pz^{\bullet-})Ru^{III}(Cl)(bpy)_2](PF_6)_2{}^* \quad (8)$$

$$[(bpy)_2(Cl)Ru^{III}(pz)Ru^{II}(Cl)(bpy)_2]^{3+} \xrightarrow{h\nu} [(bpy)_2(Cl)Ru^{II}(pz)Ru^{III}(Cl)(bpy)_2]^{3+} \quad (9)$$

An analysis was developed to explain the decrease in band energy and width in PMMA. It included the partitioning of λ_o into frozen and non-frozen parts, $\lambda_o = \lambda_{oo} + \lambda_{io}$, as described in the previous section, with a contribution from a reorganization energy arising from counter ion displacements, λ_{X^-}.

A conceptually related analysis was used to describe a ligand-based "mixed valency" and assign a low energy near-IR band in the MLCT excited-state spectrum of $[Os(phen)_3]^{2+}$ [165,166]. As shown in Eq. (10a), MLCT excitation creates a metal-bridged, ligand–ligand mixed valency. Electron transfer among the ligands in the MLCT excited state of $[Os(bpy)_3]^{2+*}$ occurs on the 10's of picoseconds timescale as shown by time-resolved polarization measurements [167].

$$Os^{II}_{{}^1(d\pi)^6}(phen)_3{}^{2+} \xrightarrow{h\nu} Os^{III}_{{}^3(d\pi)^5(\pi^*)^1}(phen^{\bullet-})(phen)_2{}^{2+*} \quad (10a)$$

$$Os^{II}(phen^{\bullet-})_a(phen)_b(phen)_c{}^{2+*} \rightarrow Os^{III}(phen)_a(phen^{\bullet-})_b(phen)_c{}^{2+*} \quad (10b)$$

Near-IR bands assigned to analogous Ligand-to-Ligand Charge Transfer (LLCT or Interligand Charge transfer

(ILCT)) transitions were previously observed in singly- and doubly-reduced $Ru(bpy)_3^{+}$ and $Ru(bpy)_3^{0}$ [168–170]. TRNIR monitoring following laser flash excitation at 450 nm of $[Os(phen)_3]^{2+}$ in CD_3CN at room temperature revealed a transient absorption feature at $\lambda_{max} = 1830$ nm ($\bar{\nu}_{max} = 5460\,cm^{-1}$) ($\varepsilon_{max} \geq 5000\,M^{-1}\,cm^{-1}$) with $\Delta\bar{\nu}_{1/2} = 1840\,cm^{-1}$. The band energy was solvent dependent consistent with a charge transfer-based transition and assigned to the LLCT transition in Eq. (10a).

Based on a detailed electronic structure model, the transient absorption feature was assigned to an overlap of three closely lying transitions. Two were of coupled $d\pi \rightarrow d\pi$ interconfigurational character because ligand–ligand charge transfer is accompanied by hole transfer among the $d\pi$ levels at Os^{III}. The band intensity was assumed to be dominated by the pure LLCT transition in Eq. (11) and an equivalent transition to ligand c. In Eq. (11), the $d\pi$ orbitals are labeled in increasing energy split by symmetry and spin-orbit coupling $\xi(Os^{III} \sim 3000\,cm^{-1})$. The symmetry labels are those for the C_{2v} symmetry of the excited state, and the lowest π^* levels on ligands a and b are labeled as π_1^*.

$$^3[(d\pi_1^2 d\pi_2^2 d\pi_3^1 \pi_{1,a}^{*\,1})] \xrightarrow{h\nu} {}^3[(d\pi_2^2 d\pi_3^1 d\pi_1^2 \pi_{1,b}^{*\,1})],$$

$$(^3[(a_1)^2(a_2)^2(b_2)^1(\pi_{1,a}^{*})^1]), \quad (^3[(a_1)^2(a_2)^1(b_2)^2(\pi_{1,b}^{*})^1]) \quad (11)$$

6. New directions and concluding remarks

Application of TRIR, especially when combined with other transient measurements, has become a powerful tool for characterizing metal complex excited states. In the future, TRIR combined with DFT and improvements in computing power, use of anharmonic treatment of vibrations, and application of solvent models, will give increasingly detailed insight into excited states and their reactions. Application of the technique across the entire IR region will become more routine and extend its usefulness.

An important extension will come in the far-IR or THz region of the spectrum. Spectroscopic information in this region is rich but, as yet, not fully interpreted. The low frequency absorptions that occur in this region may give insight into coupling of surrounding medium modes with transiently induced charge-transfer processes, with metal complex excited states, and with electron and energy transfer in molecular assemblies.

The technology underpinning TRIR continues to evolve with at least four commercial suppliers of nanosecond time-resolved spectrometers. With advances in ultra-fast laser technology and array IR detection, the components required for construction of femtosecond/picosecond transient IR spectrometers are more readily available. There have been advances in other areas of time-resolved spectroscopy particularly in the use of time-resolved X-ray crystallography [171], EXAFS [172], and electron diffraction [173] to study transients which, when exploited in combination with TRIR, will provide a powerful suite of probes for excited-state structure.

Transient non-linear 2D infrared (T2D-IR) spectroscopy on the picosecond timescale is making significant inroads with application to *fac*-[Re(dmb)(CO_3)(Cl)] mentioned in Section 3.2. As noted there, it is the infrared analogue of COSY and NOESY NMR methods and offers fast time resolution (picosecond), and direct information about the coupling of vibrational modes in transients.

The coupling of IR imaging with step-scan FT-IR methods on the millisecond to nanosecond timescales will almost certainly become a useful tool in the near term in a variety of fields from biology and biophysics, to materials science, and nanotechnology.

Acknowledgments

The authors are grateful for the many collaborations and collaborators they have had over the last decade, bringing challenging photophysical systems to the table for the application of transient infrared methods. The work at the University of North Carolina (T.J.M., D.M.D) was supported by the Chemical Sciences, Geosciences and Biosciences Division of the Office of Basic Energy Sciences, U.S. Department of Energy. D.M.D. is also grateful for a Director's funded fellowship at Los Alamos National Laboratory. Work at LANL was supported by the Laboratory's Directed Research and Development program, and the DOE/NNSA. Los Alamos National Laboratory is operated by Los Alamos National Security (LANS) LLC, for the Department of Energy.

References

[1] J.R. Schoonover, G.E. Strouse, Chem. Rev. 98 (1998) 1335.
[2] J.J. Turner, M.W. George, I.P. Clark, I.G. Virrels, Laser Chem. 19 (1999) 245.
[3] D.C. Grills, M.W. George, in: J.M. Chalmers, P.R. Griffiths (Eds.), Handbook of Vibrational Spectroscopy, 1, John Wiley & Sons, 2002, p. 677.
[4] M. Poliakoff, E. Weitz, Adv. Organomet. Chem. 25 (1986) 277–316.
[5] T.A. Heimer, E.J. Heilweil, Bull. Chem. Soc. Japan 75 (2002) 899.
[6] See special issue in J. Phys. Chem. A 104 (2000).
[7] M. Adelt, M. Devenney, T.J. Meyer, D.W. Thompson, J.A. Treadway, Inorg. Chem. 37 (1998) 2616.
[8] M.W. George, J.J. Turner, Coord. Chem. Rev. 177 (1998) 201.
[9] S. Bernhard, K.M. Omberg, G.F. Strouse, J.R. Schoonover, Inorg. Chem. 39 (2000) 3107.
[10] J.R. Schoonover, C.A. Bignozzi, T.J. Meyer, Coord. Chem. Rev. 165 (1997) 239.
[11] W. Uhmann, A. Becker, C. Taran, F. Siebert, Appl. Spectrosc. 45 (1991) 390.
[12] R.A. Palmer, V.G. Gregoriou, J.L. Chao, Polym. Prepr. 33 (1992) 1222.
[13] G.D. Smith, M.S. Hutson, Y. Lu, M.T. Tierney, M.W. Grinstaff, R.A. Palmer, Appl. Spec. 55 (2001) 637.
[14] D.M. Dattelbaum, T.J. Meyer, Introduction to Step-Scan FT-IR, Bruker Optics, Billerica, MA, 2000, 21.
[15] G.D. Smith, B.M. Paegel, R.A. Palmer, P.Y. Chen, K.M. Omberg, T.J. Meyer, Laser Chem. 19 (1999) 291.
[16] T.J. Jiao, Z. Pang, T.J. Burkey, R.F. Johnston, T.A. Heimer, V.D. Kleiman, E.J. Heilweil, J. Am. Chem. Soc. 121 (1999) 4618.
[17] J. Bredenbeck, J. Helbing, P. Hamm, J. Am. Chem. Soc. 126 (2004) 990.

[18] M. Towrie, A. Gabrielsson, P. Matousek, A.W. Parker, A.M.B. Rodriguez, A. Vlcek, Appl. Spectrosc. 59 (2005) 467.
[19] R.P.S.M. Lobo, J.D. LaVeigne, D.H. Reitze, D.B. Tanner, G.L. Carr, Rev. Sci. Instrum. 73 (2002) 1.
[20] R.A. Palmer, G.D. Smith, V.N. Litvinenko, G. Edwards, Proc. SPIE Int. Soc. Opt. Eng. 3775 (1999) 137.
[21] R.A. Palmer, G.D. Smith, P.Y. Chen, Vibrational Spectrosc. 19 (1999) 131.
[22] M.S. Hutson, R.A. Palmer, A. Gillikin, M.S. Chang, V.N. Litvinenko, G.S. Edwards, Proc. SPIE – Int. Soc. Opt. Eng. 4633 (2002) 225.
[23] M.S. Hutson, R.A. Palmer, M.S. Chang, A. Gillikin, V. Litvinenko, G. Edwards, Nucl. Instrum. Methods Phys. Res., Sect. A (Accelerators, Spectrometers, Detectors and Associated Equipment) 483 (2002) 560.
[24] D.M. Dattelbaum, K.M. Omberg, J.R. Schoonover, R.L. Martin, T.J. Meyer, Inorg. Chem. 41 (2002) 6071.
[25] D.M. Dattelbaum, K.M. Omberg, J.R. Schoonover, T.J. Meyer, Inorg. Chem. 41 (2001) 6071.
[26] D.M. Dattelbaum, T.J. Meyer, J. Phys. Chem. A. 106 (2002) 4519.
[27] D.R. Gamelin, M.W. George, P. Glyn, F.-W. Grevels, F.P.A. Johnson, W. Klotzbucher, S.L. Morrison, G. Russell, K. Schaffner, J.J. Turner, Inorg. Chem. 33 (1994) 3246.
[28] J. Wachtveitl, S. Sporlein, H. Satzger, B. Fonrobert, C. Renner, R. Behrendt, D. Oesterhelt, L. Moroder, W. Zinth, Biophys. J. 86 (2004) 2350.
[29] D.M. Dattelbaum, P.J. Hay, K.M. Omberg, N. Gebhart, R.L. Martin, B. Loeb, C.A. Bignozzi, J.R. Schoonover, T.J. Meyer, J. Phys. Chem. A 108 (2004) 3518.
[30] W.D. Bates, P.Y. Chen, D.M. Dattelbaum, W. Jones, T.J. Meyer, J. Phys. Chem. A 103 (1999) 5227.
[31] J.R. Schoonover, K.C. Gordon, R. Argazzi, W.H. Woodruff, K.A. Peterson, C.A. Bignozzi, R.B. Dyer, T.J. Meyer, J. Am. Chem. Soc. 115 (1993) 10996.
[32] M.K. Kuimoya, M.Y. Mel'nikov, J.A. Weinstein, M.W. George, J. Chem. Soc. Dalton Trans. (2002) 2857.
[33] Y.A. Kovelenov, A.J. Blake, M.W. George, P. Matousek, M.Y. Mel'Nikov, A.W. Parker, X.-Z. Sun, M. Towrie, J.A. Weinstein, Dalton Trans. (2005) 2092.
[34] R. Lopez, A.M. Leiba, F. Zuloaga, B. Loeb, B. Norambuena, K.M. Omberg, J.R. Schoonover, D.R. Striplin, M. Devenney, T.J. Meyer, Inorg. Chem. 38 (1999) 2924–2930.
[35] J. Dyer, C.G. Coates, M. Creely, J.D. Gavey, D.C. Grills, S. Hudson, W.J. Blau, J.M. Kelly, P. Matousek, J.J. McGarvey, J. McMaster, A.W. Parker, M. Towrie, J.A. Weinstein, M.W. George, Photochem. Photobiol. Sci. 2 (2003) 542.
[36] B.D. Rossenaar, M.W. George, F.P.A. Johnson, D.J. Stufkens, J.J. Turner, A. Vlcek Jr., J. Am. Chem. Soc. 117 (1995) 11582.
[37] M.P. Aarnts, M.P. Wilms, D.J. Stufkens, E.J. Baerends, A. Vlcek, I.P. Clark, M.W. George, J.J. Turner, Chem. Eur. J. 2 (1996) 1556.
[38] J.P. Claude, K.M. Omberg, D.S. Williams, T.J. Meyer, J. Phys. Chem. A 106 (2002) 7795.
[39] F.P.A. Johnson, M.W. George, S.L. Morrison, J. Chem. Soc. Chem. Comm. (1995) 391.
[40] M.W. George, F.P.A. Johnson, J.J. Turner, J. Chem. Soc. Dalton Trans. (1995) 2711.
[41] L.C. Abbott, C.J. Arnold, T.-Q. Ye, K.C. Gordon, R.N. Perutz, R.E. Hester, J.N. Moore, J. Phys. Chem. A 102 (1998) 1252.
[42] M.K. Kuimova, A.J. Cowan, P. Matousek, A.W. Parker, X.-Z. Sun, M. Towrie, M.W. George, Proc. Nat. Acad. Sci. 103 (2006) 2150.
[43] K.M. Omberg, J.R. Schoonover, S. Bernhard, J.A. Moss, J.A. Treadway, E.M. Kober, R.B. Dyer, T.J. Meyer, Inorg. Chem. 37 (1998) 3503.
[44] K.M. Omberg, J.R. Schoonover, J.A. Treadway, R.M. Leasure, R.B. Dyer, T.J. Meyer, J. Am. Chem. Soc. 119 (1997) 7013.
[45] P.G. Bradley, N. Kress, B.A. Hornberger, R.F. Dallinger, W.H. Woodruff, J. Am. Chem. Soc. 103 (1981) 7441.
[46] A.E. Curtright, J.K. McCusker, J. Phys. Chem. A 103 (1999) 7032.
[47] M.W. George, (unpublished results).
[48] D.J. Liard, M. Busby, P. Matousek, M. Towrie, A. Vlcek, J. Phys. Chem. A 108 (2004) 2363.
[49] T.M. Cooper, J.P. Blaudeau, B.C. Hall, J.E. Rogers, D.G. McLean, Y.L. Liu, J.P. Toscano, Chem. Phys. Lett. 400 (2004) 239.
[50] J.A. Weinstein, J. van Slageren, D.J. Stufkens, S. Zalis, M.W. George, J. Chem. Soc. Dalton Trans. (2001) 2587.
[51] A. Gabrielsson, P. Matousek, M. Towrie, F. Hartl, S. Zalis, A. Vlcek, J. Phys. Chem. A 109 (2005) 6147.
[52] D.M. Dattelbaum, R.L. Martin, J.R. Schoonover, T.J. Meyer, J. Phys. Chem. A. 108 (2004) 3518.
[53] K. Koike, N. Okoshi, H. Hori, K. Takeuchi, O. Ishitani, H. Tsubaki, I.P. Clark, M.W. George, J.J. Turner, J. Am. Chem. Soc. 124 (2002) 11448.
[54] D.A. Bardwell, F. Barigelletti, R.L. Cleary, L. Flamigni, M. Guardegli, J.C. Jeffrey, M.D. Ward, Inorg. Chem. 34 (1995) 2438.
[55] A.M.B. Rodriguez, A. Gabrielsson, M. Motevalli, P. Matousek, M. Towrie, J. Sebera, S. Zalis, A. Vlcek, J. Phys. Chem. A. 109 (2005) 5016.
[56] S. Zalis, M. Busby, T. Kotrba, P. Matousek, M. Towrie, A. Vlcek, Inorg. Chem. 43 (2004) 1723.
[57] S. Zalis, I.R. Farrell, A. Vlcek, J. Am. Chem. Soc. 125 (2003) 4580.
[58] F.W. Vergeer, P. Matousek, M. Towrie, M.L. Costa, F. Hartl, Chem. -A Eur. J. 10 (2004) 3451.
[59] A. Gabrielsson, S. Zalis, P. Matousek, M. Towrie, A. Vlcek, Inorg. Chem. 43 (2004) 7380.
[60] L.C. Abbott, C.J. Arnold, K.C. Gordon, R.E. Hester, J.N. Moore, R.N. Perutz, T.Q. Ye, Laser Chem. 19 (1999) 279.
[61] J.A. Treadway, P. Chen, T.J. Rutherford, F.R. Keene, T.J. Meyer, J. Phys. Chem. A 101 (1997) 6824.
[62] K.M. Omberg, J.R. Schoonover, T.J. Meyer, J. Phys. Chem. 101 (1997) 9531.
[63] J.R. Schoonover, A.P. Shreve, R.B. Dyer, Inorg. Chem. 37 (1998) 2598.
[64] K.A. Walters, D.M. Dattelbaum, K.D. Ley, J.R. Schoonover, T.J. Meyer, K.S. Schanze, Chem. Comm. (2001) 1834.
[65] K.A. Walters, Ph.D. Dissertation, Department of Chemistry, University of Florida, Gainesville 2000.
[66] A.S. DelNegro, S.M. Woessner, B.P. Sullivan, D.M. Dattelbaum, J.R. Schoonover, Inorg. Chem. 40 (2001) 5056.
[67] D.M. Dattelbaum, unpublished results.
[68] S. Encinas, A.F. Morales, F. Barigelletti, A.M. Barthram, C.M. White, S.M. Couchman, J.C. Jeffery, M.D. Ward, D.C. Grills, M.W. George, J. Chem. Soc. Dalton Trans. (2001) 3312.
[69] H. Adams, W.Z. Alsindi, G.M. Davies, M.B. Duriska, T.L. Easun, H.E. Fenton, J.M. Herrara, M.W. George, K.L. Ronayne, X.Z. Sun, M. Towrie, M.W. Ward, J. Chem. Soc. Dalton Trans. (2006) 39.
[70] C.E. Whittle, J.A. Weinstein, M.W. George, K.S. Schanze, Inorg. Chem. 40 (2001) 4053.
[71] M.J. Bakker, F. Hartl, D.J. Stufkens, O.S. Jina, X.-Z. Sun, M.W. George, Organometallics 21 (2000) 4310.
[72] F.W. Vergeer, M.J. Calhorda, P. Matousek, M. Towrie, F. Hartl, J. Chem. Soc. Dalton Trans. (2003) 4084.
[73] F.W. Vergeer, C.J. Kleverlaan, P. Matousek, M. Towrie, D.J. Stufkens, F.E. Hartl, Inorg. Chem. 44 (2005) 1319.
[74] T.P. Ortiz, J.A. Marshall, L.A. Emmert, J. Yang, W. Choi, A.L. Costello, J.A. Brozik, Inorg. Chem. 43 (2004) 132.
[75] M. Busby, P. Matousek, M. Towrie, I.P. Clark, M. Motevalli, F. Hartl, A. Vlcek, Inorg. Chem. 43 (2004) 4523.
[76] J. Saltiel, J. D'Agostino, E.D. Megarity, L. Metts, K.R. Neuberger, M.S. Wrighton, O.C. Zafiriou, Org. Photochem. 3 (1973) 1.
[77] J. Saltiel, G.S. Hammond, J. Am. Chem. Soc. 85 (1963) 2515.
[78] J. Saltiel, G.-E. Khalil, K.S. Schanze, Chem. Phys. Lett. 70 (1980) 233.
[79] J. Saltiel, G.R. Marchand, E. Kirkor-Kaminska, W.K. Smothers, W.B. Mueller, J.L. Charlton, J. Am. Chem. Soc. 106 (1984) 3144.
[80] J. Saltiel, A. Marinari, D.W.-L. Chang, J.C. Mitchener, E.D. Megarity, J. Am. Chem. Soc. 101 (1979) 2982.
[81] J. Saltiel, A.D. Rousseau, B. Thomas, J. Am. Chem. Soc. 105 (1983) 7631.
[82] J. Saltiel, A.S. Waller, D.F. Sears, J. Am. Chem. Soc. 115 (1993) 2453.
[83] D.M. Dattelbaum, M.K. Itokazu, N.Y.M. Iha, T.J. Meyer, J. Phys. Chem. 107 (2003) 4092.

[84] M. Busby, P. Matousek, M. Towrie, A. Vlcek, J. Phys. Chem. A 109 (2005) 3000.
[85] K. Kaneda, S. Sato, H. Hamaguchi, T. Arai, Bull. Chem. Soc. Jpn. 77 (2004) 1529.
[86] A. Shagal, R.H. Schultz, Organometallics 21 (2002) 5657.
[87] C.J. Breheny, S.M. Draper, F.W. Grevels, W.E. Klotzbucher, C. Long, M.T. Pryce, G. Russell, Organometallics 15 (1996) 3679.
[88] K.E. Erkkila, D.T. Odom, J.K. Barton, Chem. Rev. 99 (1999) 2777.
[89] M.K. Kuimoya, W.Z. Alsindi, J. Dyer, D.C. Grills, O.S. Jina, P. Matousek, A.W. Parker, P. Portius, X.Z. Sun, M. Towrie, C. Wilson, J.X. Yang, M.W. George, J. Chem. Soc. Dalton Trans. 21 (2003) 3996.
[90] M.R. Waterland, K.C. Gordon, J.J. McGarvey, P.M. Jayaweera, J. Chem. Soc. Dalton Trans. (1998) 609.
[91] P. Chen, T.J. Meyer, Chem. Rev. 98 (1998) 1439.
[92] N. Sutin, Acc. Chem. Res. 15 (1982) 275.
[93] B.S. Brunschwig, N. Sutin, Coord. Chem. Rev. 187 (1999) 233.
[94] N. Sutin, Prog. Inorg. Chem. 30 (1983) 441.
[95] G.C. Allen, N.S. Hush, Prog. Inorg. Chem. 8 (1967) 357.
[96] R.A. Marcus, J. Phys. Chem. 93 (1989) 3078.
[97] R.A. Marcus, N. Sutin, Biochim. Biophys. Acta 811 (1985) 265.
[98] G.R. Fleming, M. Cho, Ann. Rev. Phys. Chem. 47 (1996) 109.
[99] M.S. Wrighton, D.L. Morse, J. Organomet. Chem. 97 (1975) 405.
[100] J.R. Reimers, J. Zeng, N.S. Hush, J. Phys. Chem. 100 (1996) 1498.
[101] L. Vincze, D.A. Friesen, S.P. Mezyk, W.L. Waltz, Inorg. Chem. 31 (1992) 4950.
[102] D.A. Friesen, S.H. Lee, R.E. Nashiem, S.P. Mezyk, W.L. Waltz, Inorg. Chem. 34 (1995) 4026.
[103] F. de Buyl, A.K. Mesmaeker, J. Photochem. Photobiol. A 60 (1991) 27.
[104] P. Chen, S.L. Mecklenburg, R. Duesing, T.J. Meyer, J. Phys. Chem. 97 (1993) 6811.
[105] J.V. Caspar, Ph.D. Dissertation, Department of Chemistry, The University of North Carolina at Chapel Hill, Chapel Hill, NC 1982.
[106] J.V. Caspar, T.J. Meyer, J. Am. Chem. Soc. 105 (1983) 5583.
[107] C.J. Timpson, C.A. Bignozzi, B.P. Sullivan, E.M. Kober, T.J. Meyer, J. Phys. Chem. 100 (1996) 2915.
[108] A.J. Lee, Comments Inorg. Chem. 17 (1995) 319.
[109] P. Chen, T.J. Meyer, Inorg. Chem. 35 (1996) 5520.
[110] I.P. Clark, M.W. George, F.P.A. Johnson, J.J. Turner, Chem. Comm. (1996) 1587.
[111] P.J. Giordano, S.M. Fredericks, M.S. Wrighton, D.L. Morse, J. Am. Chem. Soc. 100 (1978) 5051.
[112] P.J. Giordano, M.S. Wrighton, J. Am. Chem. Soc. 101 (1979) 2888.
[113] G.D. Hager, G.A. Crosby, J. Am. Chem. Soc. 97 (1975) 7031.
[114] G.A. Crosby, R.G. Highland, K.A. Truesdell, Coord. Chem. Rev. 64 (1985) 41.
[115] J.A. Burt, G.A. Crosby, Chem. Phys. Lett. 220 (1994) 493.
[116] S.M. Fredericks, J.C. Luong, M.S. Wrighton, J. Am. Chem. Soc. 101 (1979) 7415.
[117] K.J. Jordan, W.F. Wacholtz, G.A. Crosby, Inorg. Chem. 30 (1991) 4588.
[118] J.F. Endicott, R.B. Lessard, D. Lynch, M.W. Perkovic, C.K. Ryu, Coord. Chem. Rev. 97 (1990) 65.
[119] P.Y. Chen, T.D. Westmoreland, E. Danielson, K.S. Schanze, D. Anthon, P.E. Neveux, T.J. Meyer, Inorg. Chem. 26 (1987) 1116.
[120] J.P. Claude, Ph.D. Dissertation, Department of Chemistry, University of North Carolina, Chapel Hill, NC (1995) 191.
[121] J.P. Claude, D.S. Williams, T.J. Meyer, J. Am. Chem. Soc. 118 (1996) 9782.
[122] K.S. Schanze, K.A. Walters, in: V. Ramanurthy, K.S. Schanze (Eds.), Molecular and Supramolecular Photochemistry, Vol. 2, Marcel Dekker, New York, 1998.
[123] D.J. Stufkens, A. Vlcek, Coord. Chem. Rev. 177 (1998) 127.
[124] M.S. Wrighton, D.L. Morse, J. Am. Chem. Soc. 96 (1974) 998.
[125] S.M. Baxter, W.E. Jones, E. Danielson, L.A. Worl, G.F. Strouse, J. Younathan, T.J. Meyer, Coord. Chem. Rev. 111 (1991) 47.
[126] G.D. Smith, M.S. Hutson, Y. Lu, M.T. Tierney, M.W. Grinstaff, R.A. Palmer, Appl. Spectrosc. 55 (2001) 637.
[127] D.G. Thompson, J.F. Wishart, B.S. Brunschwig, N. Sutin, J. Phys. Chem. A 105 (2001) 8117.
[128] S. Tachiyashiki, K. Mizumachi, Coord. Chem. Rev. 132 (1994) 113.
[129] D.P. Rillema, C.B. Blanton, R.J. Shaver, D.C. Jackman, M. Boldaji, S. Bundy, L.A. Worl, T.J. Meyer, Inorg. Chem. 31 (1992) 1600.
[130] D.P. Rillema, D.G. Taghdiri, J.S. Jones, C.D. Keller, L.A. Worl, T.J. Meyer, H.A. Levy, Inorg. Chem. 26 (1987) 578.
[131] W.F. Wacholtz, R.A. Auerbach, R.H. Schmehl, Inorg. Chem. 25 (1986) 227.
[132] W.M. Wacholtz, R.A. Auerbach, R.H. Schmehl, M. Ollino, W.R. Cherry, Inorg. Chem. 24 (1985) 1758.
[133] F. Barigelletti, A. Juris, V. Balzani, P. Belser, A. von Zelewsky, J. Phys. Chem. 90 (1986) 5190.
[134] A. Juris, F. Barigelletti, V. Balzani, P. Belser, A. von Zelewsky, Inorg. Chem. 24 (1985) 202.
[135] G.H. Allen, R.P. White, D.P. Rillema, T.J. Meyer, J. Am. Chem. Soc. 106 (1984) 2613.
[136] D.V. Pinnick, B. Durham, Inorg. Chem. 23 (1984) 1440.
[137] W.R. Cherry, L.J. Henderson, Inorg. Chem. 23 (1984) 983.
[138] B.J. Coe, D.A. Friesen, D.W. Thompson, T.J. Meyer, Inorg. Chem. 35 (1996) 4575.
[139] L.J.J. Henderson, F.R. Fronczek, W.R. Cherry, J. Am. Chem. Soc. 106 (1984) 5867.
[140] K.R. Barqawi, A. Llobet, T.J. Meyer, J. Am. Chem. Soc. 110 (1988) 7751.
[141] R. Bhargava, I.W. Levin, Appl. Spectr. 57 (2003) 357.
[142] R. Bhargava, I.W. Levin, Macromolecules 36 (2003) 92.
[143] T.A. Heimer, E.J. Heilweil, J. Phys. Chem. B 101 (1997).
[144] N.A. Anderson, T.Q. Lian, Ann. Rev. Phys. Chem. 56 (2005) 491.
[145] J.B. Asbury, E.C. Hao, Y.Q. Wang, T.Q. Lian, Springer Ser. Chem. Phys. 66 (2001) 450.
[146] M.K. Nazeeruddin, A. Kay, I. Rodicio, R. Humphry-Baker, P. Muller, N. Liska, N. Vlachopoulos, M. Gratzel, J. Am. Chem. Soc. 115 (1993) 6382.
[147] M.K. Nazeeruddin, P. Péchy, M. Grätzel, Chem. Comm. (1997) 1705.
[148] B. O'Regan, M. Gratzel, Nature 353 (1991) 737.
[149] M.K. Nazeeruddin, M. Grätzel, K. Kalyanasundaram, R.B. Girling, R.E. Hester, J. Chem. Soc. Dalton Trans. (1993) 323.
[150] Y.Q. Wang, J.B. Asbury, T.Q. Lian, J. Phys. Chem. A 104 (2000) 4291.
[151] X. Ai, N.A. Anderson, J.C. Guo, T.Q. Lian, J. Phys. Chem. B 109 (2005) 7088.
[152] H.N. Ghosh, J.B. Asbury, T.Q. Lian, J. Phys. Chem. B 102 (1998) 6482.
[153] H.N. Ghosh, J.B. Asbury, Y.X. Weng, T.Q. Lian, J. Phys. Chem. B 102 (1998) 10208.
[154] J.B. Asbury, E.C. Hao, Y.Q. Wang, T.Q. Lian, J. Phys. Chem. B 104 (2000) 11957.
[155] E.C. Hao, N.A. Anderson, J.B. Asbury, T.Q. Lian, J. Phys. Chem. B 106 (2002) 10191.
[156] C. She, N.A. Anderson, J. Guo, F. Liu, W.H. Goh, D.T. Chen, D.L. Mohler, T. Zhong-Qun, J.T. Hupp, T.Q. Lian, J. Phys. Chem. B 109 (2005) 19345.
[157] J.W. Snyder, I. Zebger, Z. Gao, L. Poulsen, P.K. Frederiksen, E. Skovsen, S.P. McIlroy, M. Klinger, L.K. Andersen, P.R. Ogilby, Acc. Chem. Res. 37 (2004) 894.
[158] D.M. Dattelbaum, C.M. Hartshorn, T.J. Meyer, J. Am. Chem. Soc. 123 (2002) 4938.
[159] S.F. Nelsen, R.F. Ismagilov, D.A. Trieber II, Science 278 (1997) 846.
[160] S.F. Nelson, J. Adamus, J.J. Wolff, J. Am. Chem. Soc. 116 (1994) 1589.
[161] S.F. Nelson, D.A.I. Trieber, J.J. Wolff, D.R. Powell, S. Rogers-Crowley, J. Am. Chem. Soc. 119 (1997) 6873.
[162] S.F. Nelson, R.F. Ismagilov, D.R. Powell, J. Am. Chem. Soc. 119 (1998) 10213.
[163] S.F. Nelson, R.F. Ismagilov, K.E. Gentile, D.R. Powell, J. Am. Chem. Soc. 121 (1999) 7108.
[164] C.M. Elliott, D.L. Derr, D.V. Matyushov, M.D. Newton, J. Am. Chem. Soc. 120 (1998) 11714.
[165] M.V.H. Huynh, D.M. Dattelbaum, T.J. Meyer, Coord. Chem. Rev. 249 (2005) 457.
[166] D.M. Dattelbaum, E.M. Kober, J.M. Papanikolas, T.J. Meyer, Chem. Phys. 326 (2006) 71.
[167] G.B. Shaw, C.L. Brown, J.M. Papanikolas, J. Phys. Chem. A. 106 (2002) 1483.

[168] G.A. Heath, L.J. Yellowlees, P.S. Braterman, Chem. Phys. Lett. 92 (1982) 646.
[169] C.M. Elliot, J. Chem. Soc. Chem. Comm. (1980) 261.
[170] G.A. Heath, L.J. Yellowlees, P.S. Braterman, J. Chem. Soc. Chem. Comm. (1981) 287.
[171] J.M. Cole, Chem. Soc. Rev. 33 (2004) 501.
[172] C. Bressler, M. Chergui, Chem. Rev. 104 (2004) 1781.
[173] H. Ihee, V.A. Lobastov, U.M. Gomez, B.M. Goodson, R. Srinivasan, C.Y. Ruan, A.H. Zewail, Science 291 (2001) 458.